PhD Thesis Abstract

Andreea Petronela DIAC

Mémoire présenté en vue de l'obtention

du grade de Docteur de l'Université d'Angers

et

du grade de Docteur de l'Université Babeş-Bolyai

Discipline : Chimie

Spécialité : Chimie Organique

Laboratoire : Centre de Chimie Supramoléculaire Organique et Organométallique, Université Babeş-Bolyai, Cluj-Napoca

UMR CNRS 6200 Institut des Sciences et Technologies Moléculaires d'Angers, Angers

Soutenue le 21 October 2015

École doctorale : ***CCSOOM, Cluj-Napoca, Romania***

3MPL, Matière, Molécules, Matériaux en Pays de la Loire, Angers, France

Design, Synthesis and Supramolecular Architectures of New Heterocyclic Compounds with Potential Applications in Material Chemistry and Photovoltaic Conversion

JURY

Président: **Mr. Cristian SILVESTRU**, Professeur, Université Babeş-Bolyai, Cluj-Napoca, Roumanie

Rapporteurs: **Mr. Jean-Manuel RAIMUNDO**, Professeur, Université Aix-Marseille, Marseille, France

Mr. Marius ANDRUH, Professeur, Université de Bucarest, Bucarest, Roumanie

Examinateurs: **Mr. Philippe BLANCHARD**, Directeur de recherche CNRS, Université d'Angers, Angers, France

Mme. Niculina HĂDADE, Maitre de conférence, Université Babeş-Bolyai, Cluj-Napoca, Roumanie

Directeur de Thèse: **Mr. Ion GROSU**, Professeur, Université Babeş-Bolyai, Cluj-Napoca, Roumanie

Co-directeur de Thèse: **Mr. Jean RONCALI**, Directeur de recherche CNRS, Université d'Angers, Angers, France

Contents at a glance

KEYWORDS: Cyclopenta[*c*]pyrans; Indenopyrones; Fluorescence; Molecular electronics; Electron–donor; Organic Solar Cells; Carbon 'quantum' Dots; Light Emitting Diode (LED).

General Introduction

The research work presented in this thesis is focused on five main fields of interest with reference to synthesis of new: a) heterocyclic cyclopenta[*c*]pyrans; b) indenopyrone derivatives with fluorescent properties; c) architectures based on cyclopenta[*c*]pyran unit as potential devices of molecular electronics; d) systems based on *N,N'*-diphenylhydrazone and triphenylamine as molecular donors for organic photovoltaics and e) electroluminescent carbon 'quantum' dots. The first three subjects and the last were developed at Babes-Bolyai University, Cluj-Napoca, in the research group of Prof. Dr. Ion Grosu, while the subject concerning molecular donors for organic solar cells was developed at Moltech-Anjou, Angers, in the research group of D. R. Jean Roncali.

The first subject presents a study of pseudoazulene derivatives having a cyclopenta[*c*]pyran unit. The survey comprises the synthesis, structural analysis and reactivity towards electrophilic substitution in order to obtain fluorescent compounds. By following a multi-step strategy which starts from 1,3,4-oxadiazin-6-ones, six new series of cyclopenta[*c*]pyran derivatives were obtained and investigated using 1D, 2D NMR, UV-Vis/fluorescence spectroscopy, mass spectrometry, cyclic voltammetry and X-Ray diffractometry.

The second subject concerns the investigation of some new indenopyrone derivatives, including separation of regio- and diastereoisomers, study of their fluorescent properties and determination of fluorescence quantum yield.

The third subject describes the synthesis of new architectures based on cyclopenta[*c*]pyran unit that can be structurally modified by the influence of a chemical or electrochemical stimulus in order to work as potential devices in molecular electronics.

The fourth subject describes the synthesis of new Donor–Acceptor molecules (D–π–A) built by connecting a diphenylhydrazone block to a dicyanovinyl acceptor group via various thiophene–based π-conjugating spacers. Furthermore, new ADDA and ADADA systems based on triphenylamine as molecular donors for organic solar cells (OSCs) were obtained. The study comprises also a characterization of their electronic properties by UV-Vis absorption spectroscopy, cyclic voltammetry and a preliminary evaluation of their performances in OSCs.

The fifth and last subject outlines the passivation of surface defects on carbon nanoparticles using small organic molecules or polymers in order to obtain photoluminescent carbon nanoparticles dubbed as carbon'quantum'dots. Moreover, the potential of carbon dots to function as energy donors by covalently attaching rhodamine B (RhB) to the free amino group of CDs-PEG_{1500N} and the electroluminescence properties of carbon dots in a LED device were investigated.

Chapter 1: Design, Synthesis and Analysis of New Fluorescent Cyclopenta[*c*]pyrans

1.1. Introduction

The cyclopenta[*c*]pyrans are aromatic compounds consisting of one cyclopentadiene fused at the *c*-bond of a pyran unit (**A1**, chart 1). The aromatic character of these derivatives is given by the total number of 10 conjugated π-electrons including the lone pair of the oxygen atom.[1] The parent compound **A1** belongs to a large class of heterocyclic compounds, namely pseudoazulenes[2], which are π-isoelectronic analogues of the non-benzenoid aromatic hydrocarbon azulene. Formally, the cyclopenta[*c*]pyran moiety results by replacing a vinylene group at C-5–C-6 position of azulene **A2** by an oxygen atom (chart 1).

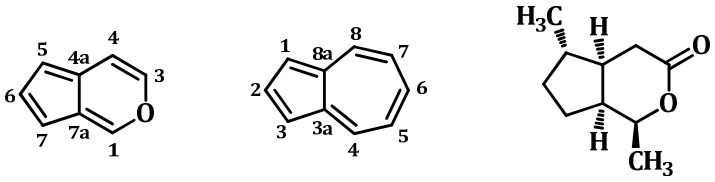

A1 **A2** **A3**

Chart 1

The cyclopenta[*c*]pyran scaffold appears as the subunit or the core of many natural products called *Iridoids*.[3] The name „iridoids" given after the first member iridomyrmecin derivative **A3** was isolated in 1949 by Pavan[4] from the secretion of ants belonging to the genus *Iridomyrmex*, species *Iridomyrmex humilis*. This proved to be an effective insecticide and has antibiotic activity. Furthermore, iridoids are monoterpenes, often found as intermediates in the biosynthesis of alkaloids. Having a partially or fully hydrogenated cyclopenta[*c*]pyran skeleton, they attracted considerable attention due to their divers and important biological activities.[1,3,5,6,7,8,9]

---

[1] M. Ţînţaş, E. Bogdan, I. Grosu, *J. Heterocycl. Chem*. **2011**, *48*, 747.
[2] H.-J. Timpe, A.V. El'tsov, *Adv. Heterocycl. Chem.* **1983**, *33*, 185.
[3] A. Nangia, G. Prasuna, P.B. Rao, *Tetrahedron* **1997**, *53*, 14507.
[4] M. Pavan, *Ric. Sci.* **1949**, *19*, 101.
[5] S. Isoe, *Stud. Nat. Prod. Chem.* **1995**, *16*, 289.
[6] X. Wei, H. Xie, X. Ge, F. Zhang, *Phytochemistry* **2000**, *53*, 837.
[7] K. H. Shaker, M. H. A. Elgamal, K. Seifert, *Z. Naturforsch* **2001**, *56C*, 965.
[8] H. Y. Hsu, J. J. Yang, C. C. Lin, *Cancer Lett.* **1997**, *113*, 31.
[9] F. E. Koehn, S. P. Gunasekara, D. N. Niel, S. S. Cross, *Tetrahedron Lett.* **1991**, *32*, 169.

1.2. Original contributions

This chapter presents a study of pseudoazulene derivatives possessing a cyclopenta[*c*]pyran moiety. The survey comprises the synthesis, structural analysis and reactivity towards electrophilic substitution reactions in order to obtain compounds with fluorescent properties.

Different strategies to enhance the stability of aromatic cyclopenta[*c*]pyrans were investigated over time because of their sensitivity to air, strong acidic or alkaline media.

Employing the method developed by Christl[10], the synthesis of a series of new aromatic cyclopenta[*c*]pyran derivatives was performed as depicted in the retrosynthetic scheme 1.

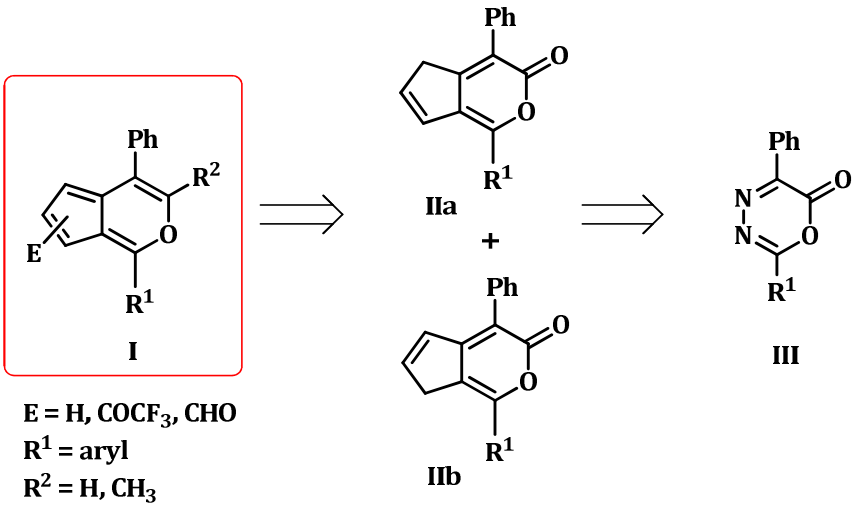

Scheme 1

The obtained cyclopenta[*c*]pyrans are intense colored compounds, some of them presenting fluorescence in solution and in solid state.

1.2.1. Synthesis of 3,4,4a,5-tetrahydrocyclopenta[*c*]pyran-3-ones

The key-step of the proposed strategy, when the cyclopenta[*c*]pyran skeleton is formed,[11]is the *inverse-electron-demand* Diels-Alder reaction. The 1,4-addition of cyclopentadiene monomer (diene component) to oxadiazinones **1**[12] (dienophile components) occurs under acidic conditions, in presence of TFA and TFAA, leading to enol-

[10] M. Christl, N. Bien, G. Bodenschatz, E. Feineis, J. Hegmann, C. Hofmann, S. Mertelmeyer, J. Ostheimer, F. Sammtleben, S. Wehner, E.-M. Peters, K. Peters, M. Pfeiffer, D. Stalke, *Chem. Commun.* **1998**, *21*, 2387.

[11] E. Feineis, H. Schwarz, J. Hegmann, M. Christl, E.-M. Peters, *Chem. Ber*. **1993**, *126*, 1743.

[12] M. L. Tintas, A. P. Diac, A. Soran, A. Terec, I. Grosu, E. Bogdan, *J. Molec. Struct*. **2014**, *1058*, 106.

lactones, 3,4,4a,5-tetrahydrocyclopenta[*c*]pyran-3-ones, as a mixture of isomers **2** and **3** (scheme 2, in red-the new derivatives). The diazalactone derivatives **1** were obtained in good yields using a known procedure.[12]

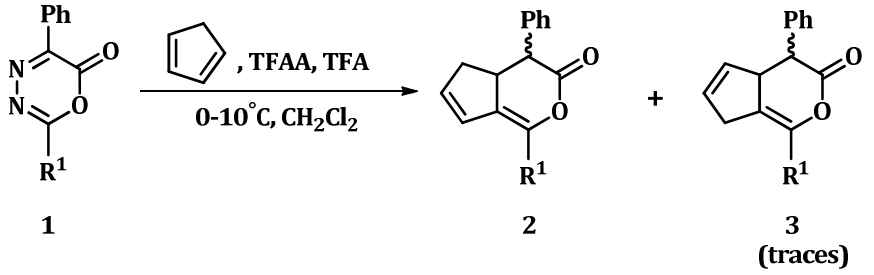

2 a $R^1 = C_6H_5$	**75%**
b $R^1 = C_6H_4$-*p*-CH_3	**65%**
c $R^1 = C_6H_4$-*p*-OCH_3	**80%**
d $R^1 = C_6H_4$-*p*-Cl	**59%**
e $R^1 = C_6H_4$-*p*-Br	**76%**
f $R^1 = C_6H_4$-*p*-*t*Bu	**67%**
g $R^1 = C_6H_4$-*m*-OCH_3	**54%**
h $R^1 = C_6H_4$-*m*-Cl	**46%**
i $R^1 = C_6H_4$-*m*-Br	**43%**
j $R^1 = C_6H_4$-*p*-NO_2	**40%**

Scheme 2

The ^{1}H NMR spectra and TLC analysis revealed the formation of several products; therefore the cycloaddition does not occur selectively. Theoretically, two regioisomers can be formed: the isomer **2,** which exhibits the double bond at C-6–C-7 and its regioisomer **3** having the double bond at C-5–C-6. Each regioisomer presents a set of diastereoisomers (**2'/3'** possessing the two hydrogen atoms at positions 4 and 4a in a *trans* configuration and **2''/3''** having the two hydrogen atoms in a *cis* configuration) (chart 2).

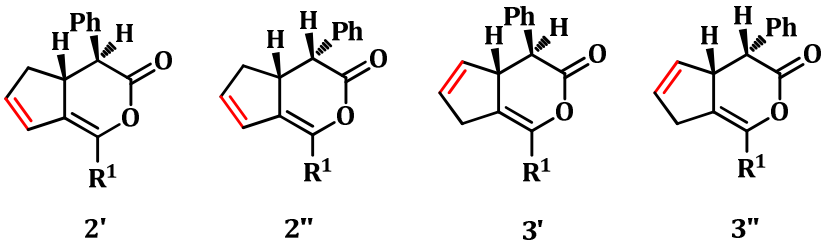

Chart 2. Possible isomers of enol-lactone derivatives

In fact, in most cases, formation of **3** is not observed, the regioisomer **2** being the major product. The ratio between the diastereoisomers **2'/2''** depends on the substituent's nature.

The separation of diastereoisomers was not possible by conventional chromatography (except for derivatives **c**, **e** and **g**) because they exhibit very close retention factor even in less polar eluent. Nevertheless, the successful isolation of diastereoisomers **2'** as individual isomer has been achieved (in very small amounts) for all substituents.

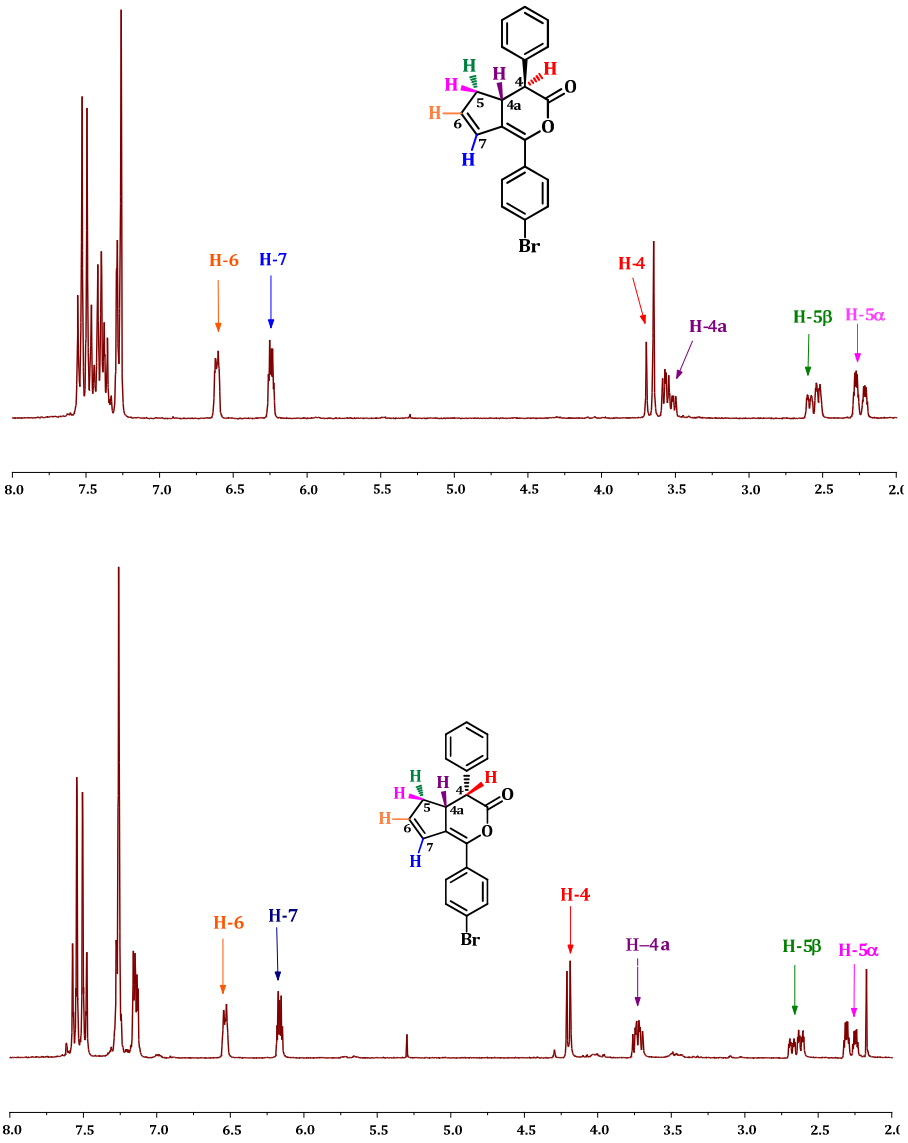

Figure 1. Fragments of ^{1}H NMR spectra (300 MHz, $CDCl_3$) of isomer **2'e** (top) and isomer **2''e** (bottom).

The configuration of the two diastereoisomers **2'e** and **2''e** (R^1=C_6H_4-*p*-Br) was determined by ^{1}H NMR spectroscopy (figure 1). For the isomer **2'e**, the large coupling constant ($J_{4,4a}$ = 14.5 Hz) indicated the *trans* disposition of H–*4* relative to H–*4a*, while in isomer **2''e** the proton H-*4* exhibits a more deshielded doublet with a coupling constant ($J_{4,4a}$ = 7.0 Hz) characteristic for the *cis* configuration.

The electrochemical properties of some compounds have been analyzed by cyclic voltammetry (CV) in methylene chloride as solvent and in presence of

tetrabutylammonium hexafluorophosphate (Bu_4NPF_6) as supporting electrolyte. The CV of all derivatives shows an irreversible oxidation wave with an anodic peak potential E_{pa} decreasing from 1.56 V for **2'j** to 1.29 V for **2'b** (Table 1, Figure 2). A closer examination of the CVs shows that the presence of electron-donating groups as $–OCH_3$, $-CH_3$, $C(CH_3)_3$ produces a large negative shift of the anodic peak potential from 1.56 V for derivative **2'j** possessing a strong EWG ($-NO_2$) to 1.29 V for compound **2'b** having an EDG ($-CH_3$) (table 1). Noteworthy, there are no differences between the stereoisomers regarding the oxidation and reduction processes.

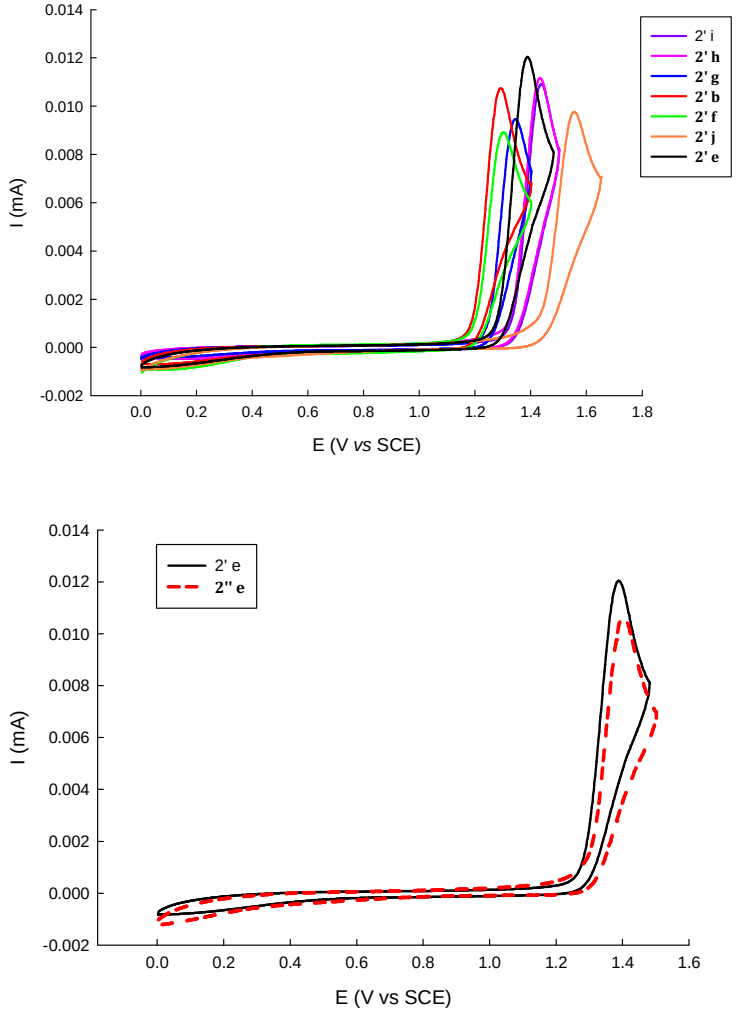

Figure 2. Cyclic voltammograms corresponding to the oxidation of enol-lactones **2b, e-j** (top) and **2'e** *vs.* **2''e** (bottom) in 0.10 M Bu_4NPF_6/CH_2Cl_2, Pt electrodes, scan rate 100 mVs^{-1}.

The CV recorded in the negative potentials region shows that all compounds present an irreversible reduction wave with a cathodic peak potential varying from -1.25 V for derivative **2'g** to –1.08 V for **2'f**. In the case of derivative **2'j** the cathodic peak potential

(E_{pc}) is positively shifted by *ca*. 100 mV and becomes reversible (table 1). Therefore, the EWG, NO_2, allows a better delocalization of negative charges in compound **2'j.**

Table 1. Cyclic voltammetry data for compounds **2b**, **2e-j** in 0.1 M Bu_4NPF_6/CH_2Cl_2, scan rate 100 mV/s, reference SCE

Cmpd.	E_{pa} (V)	E_{pc} (V)	**Cmpd.**	E_{pa} (V)	E_{pc} (V)
2'b	1.29	-1.10	**2'g**	1.35	-1.25
2'e	1.39	-1.24	**2'h**	1.43	-1.21
2''e	1.40	-1.18	**2'i**	1.43	-1.21
2'f	1.30	-1.08	**2'j**	1.56	-1.14

The optoelectronic properties of enol-lactone derivatives **2** were also investigated. The UV-Vis spectra (figure 3) of 3,4,4a,5-tetrahydrocyclopenta[*c*]pyran-3-one derivatives **2** performed in dichloromethane showed absorption maxima at around 230 and 290–305 nm (table 2) in case of all derivatives, except for compound **2'j** (R = C_6H_4-*p*-NO_2). For the latter, a notable red shift (63 nm) to λ_{max} = 361 nm could be observed. This feature could be related to the extended conjugation of the system due to the presence of the NO_2 group.

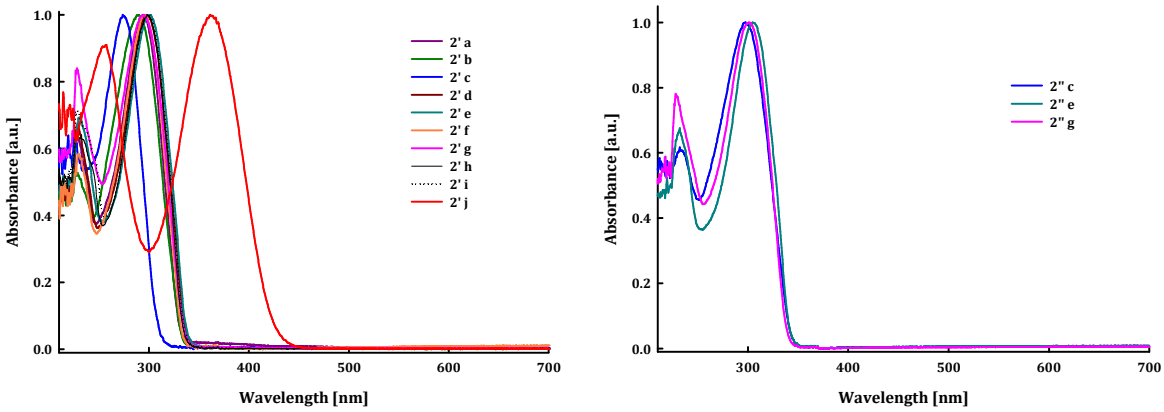

Figure 3. Normalized absorption spectra of *trans* (left) and *cis* derivatives **2** (right) recorded in CH_2Cl_2 at room temperature

The photoluminescence properties of compounds **2** have been analyzed in both solution and solid state (for some derivatives). All derivatives **2a–i** displayed a blue emission in dichloromethane solution and in solid state, in both cases the excitation wavelength being 370 nm (figure 4, table 2). By excitation at the maximum absorption wavelength, the enol-lactones **2** did not display any emission. It is important to note that compound **2'j** fluoresce in both solution and solid state with yellow emission peak at 547 nm and 533 nm, respectively.

Table 2. Absorption and emission data for 3,4,4a,5-tetrahydrocyclopenta[*c*]pyran-3-one derivatives **2**

Cmpd.	λ (nm)[a]	ε_{max} ($M^{-1}cm^{-1}$)	λ_{em} (nm)[b]	λ_{em} (nm)[c]	Φ_{FL} (%)[d]
2'a	229, *294*	16806	416, 443 (*sh*), 530 (*sh*)	-	16
2'b	228, *290*	26685	416, 439 (*sh*), 532 (*sh*)	-	3
2'c	229, *290*	9826	416, 439 (*sh*), 532 (*sh*)	-	5
2''c	232, *297*	22130	405, 540 (*sh*)	-	0.1
2'd	230, *298*	19191	416, 439 (*sh*), 548 (*sh*)	-	9
2'e	230, *302*	19858	416, 439 (*sh*), 544 (*sh*)	454	1
2''e	232, *305*	16769	410, 430, 540 (*sh*)	470	5
2'f	230, *295*	15818	416, 439 (*sh*), 538 (*sh*)	450	0.4
2'g	228, *294*	16323	416, 432 (*sh*), 535 (*sh*)	-	3
2''g	228, *302*	15049	452, 532 (*sh*)	-	6
2'h	228, *298*	15796	416, 440 (*sh*), 540 (*sh*)	440	1
2'i	228, *299*	19676	416, 440 (*sh*), 533 (*sh*)	445	0.3
2'j	257, *361*	12770	496 (*sh*), 547	533	28[e]

[a] UV-Vis absorption wavelengths in dichloromethane at room temperature
[b] Fluorescence wavelengths in dichloromethane at room temperature
[c] Fluorescence wavelengths in solid state at room temperature
[d] Fluorescence quantum yields measured in CH_2Cl_2 solution using a 0.5 M H_2SO_4 solution of quinine sulfate (Φ_{FL} = 0.54) as reference
[e] Fluorescence quantum yield measured in CH_2Cl_2 using a solution of rhodamine 123 in ethanol (Φ_{FL} = 0.96) as reference

Compared to the diluted CH_2Cl_2 solutions, the emission spectra in solid state of some compounds (figure 4) showed a better–resolved vibrational fine structure and shifts to longer wavelengths by 24–37 nm. The red shift of the emission observed in the solid state is probably due to the strong intermolecular forces, which drove the molecules to pack at high density and form *J*-aggregates. The low quantum yields determined using quinine sulfate as reference standard, suggest a prominent nonradiative deactivation pathway for the excited state.

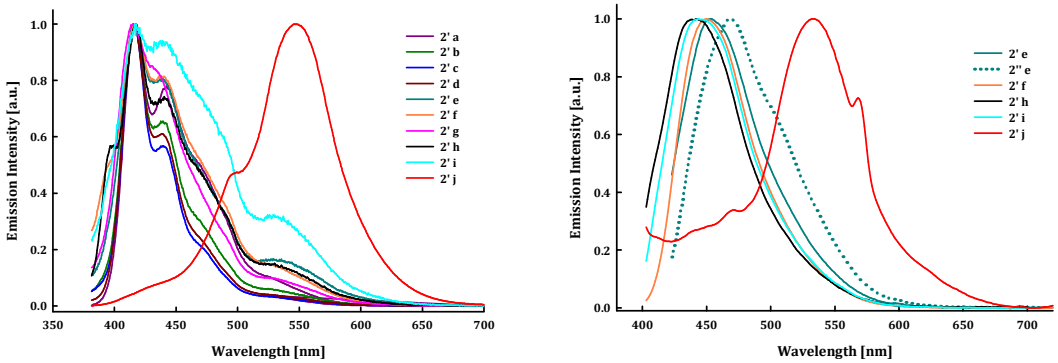

Figure 4. Normalized fluorescence spectra of enol-lactones **2** recorded in CH_2Cl_2 solution (left) and solid state (right) by excitation at 370 nm at room temperature

The molecular structure of four enol-lactones (**2''c**, **2'd**, **2'e**, **2'h**) was confirmed by X-ray diffractometry. Colorless crystals were obtained by slow evaporation from chloroform solution.

As shown in figure 5, the hydrogen atoms connected to the stereo centers C-7–C-8, and C-6–C-7, respectively, in compounds **2'd**, **2'e** and **2'h** are disposed in a *trans* configuration, while for the derivative **2''c** the X-Ray diffraction analysis confirms the *cis* orientation of the hydrogen atoms H-2–C-2–C-3–H-3.

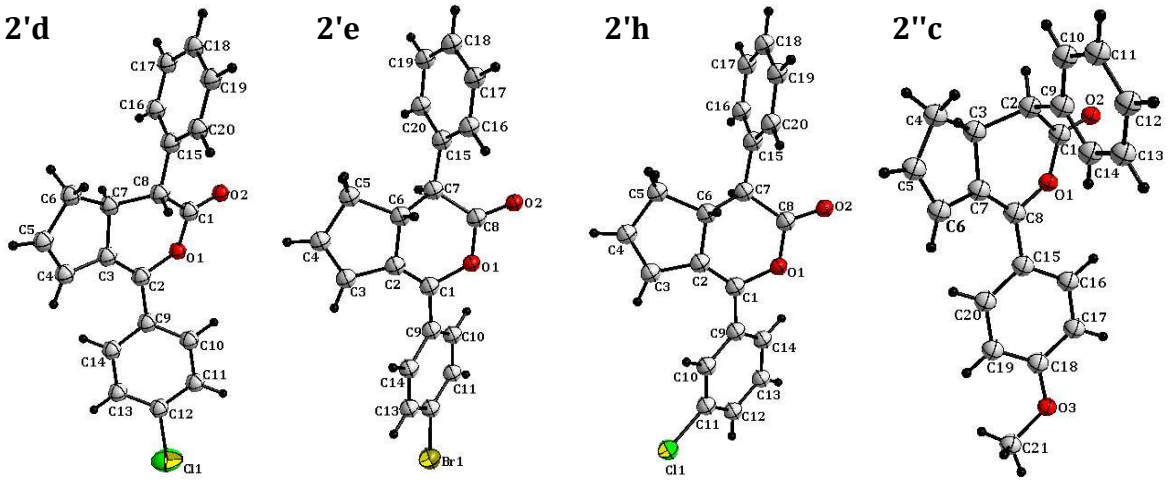

Figure 5. Single crystal molecular structure of compounds **2'd**, **2'e**, **2'h**, **2''c**

1.2.2. Synthesis of 1,4-diaryl-dihydrocyclopenta[*c*]pyrans

The synthesis of 1,4-diaryl-dihydrocyclopenta[*c*]pyran derivatives **4** and **5** was carried out in good yields by dehydrogenation of the enol-lactone isomeric mixture **2** in presence of DDQ, at reflux in chloroform (scheme 2, in red–the new compounds).[10] After the oxidation was complete a regioisomeric mixture of α-pyrones was identified.

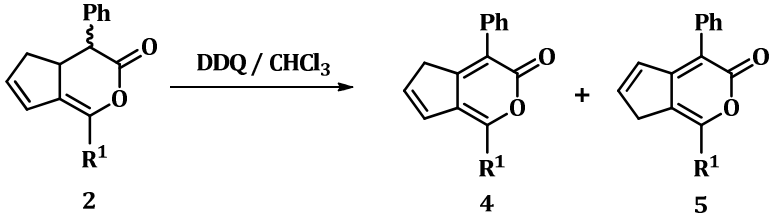

a $R^1 = C_6H_5$ 69%
b $R^1 = C_6H_4$-*p*-CH_3 62%
c $R^1 = C_6H_4$-*p*-OCH_3 74%
d $R^1 = C_6H_4$-*p*-Cl 36%
e $R^1 = C_6H_4$-*p*-Br 70%
f $R^1 = C_6H_4$-*p*-*t*Bu 52%
g $R^1 = C_6H_4$-*m*-OCH_3 48%
h $R^1 = C_6H_4$-*m*-Cl 32%
i $R^1 = C_6H_4$-*m*-Br 21%

Scheme 3

Purification of α-pyrones on silica gel led to a mixture of isomers **4** and **5**, but when neutral aluminum oxide was used for purification by column chromatography, the

isomerisation process of **4** to **5** occurred (scheme 4). This isomerisation took place with partial degradation of the product, which explains the low yield (about 25%).

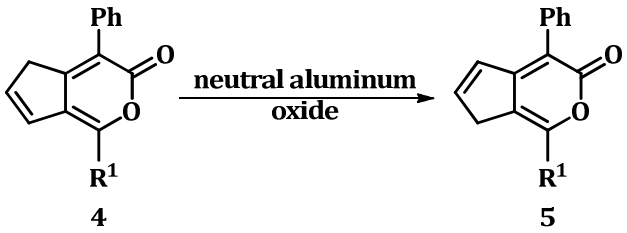

Scheme 4

The structures of α-pyrone derivatives were investigated by NMR, UV-Vis and fluorescence spectroscopy, mass spectrometry and in some cases by X-Ray diffractometry. The ^{1}H NMR spectra of derivatives **4** and **5** exhibit specific signals for the protons of vinylene unit in the range 6.3–7.0 ppm and for the protons of methylene group at position 5 and 7, respectively. The assignment of the signals was based on two-dimensional spectra and the two regioisomers were identified based on the signals of the cyclopenta[*c*]pyran protons at positions 5, 6 and 7 as illustrated in figure 6 for derivatives **4g** and **5g** (R^1 = C_6H_4-*m*-OCH_3).

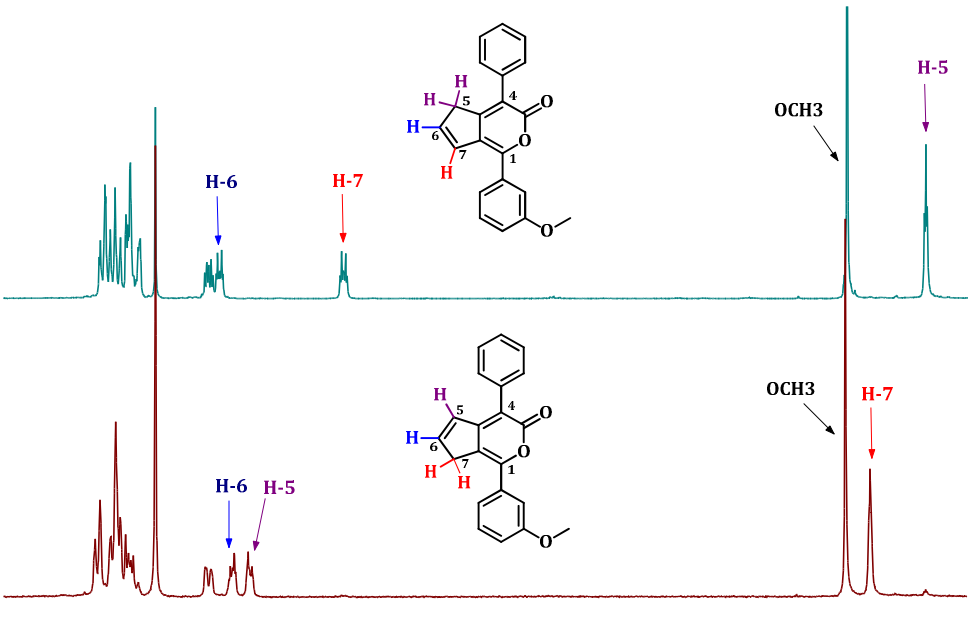

Figure 6. Fragments of ^{1}H NMR (300 MHz, $CDCl_3$) spectra of derivatives **4g** (top) and **5g** (bottom)

Dihydrocyclopenta[*c*]pyrans **4** and **5** are intense yellow solids, behavior illustrated by absorption maxima in the range 366–382 nm in the UV-Vis spectra (figure 7). The UV-

Vis and fluorescence spectra were recorded in dichloromethane solution at room temperature.

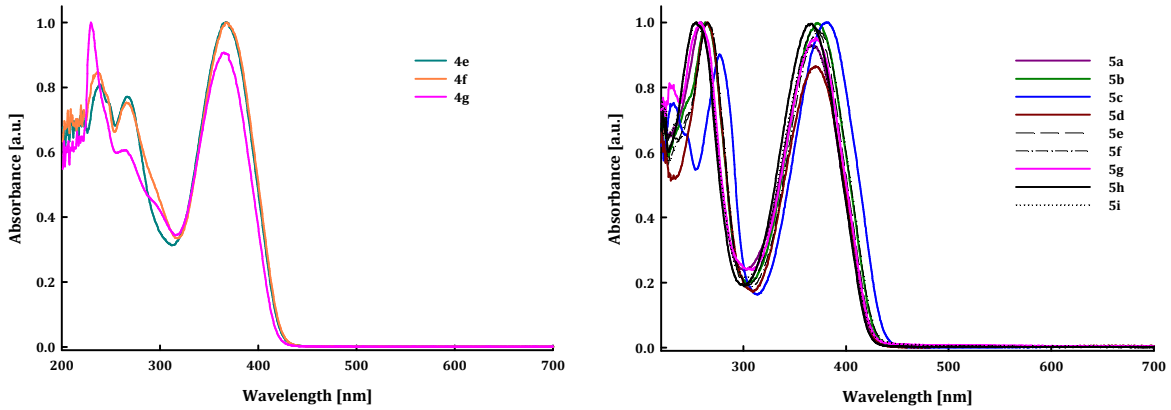

Figure 7. Absorption spectra of dihydrocyclopenta[*c*]pyrans **4** and **5** in dichloromethane

All compounds exhibit strong absorptions maxima around 366–382 nm in CH_2Cl_2 solutions, range that may be assigned to π–π* transitions. As it can be observed in figure 7, isomers **4** exhibit only one intense band with two weak shoulders, while isomers **5** exhibit two different intense bands, typical for n–π* and π–π* transitions.

The photoluminescence property of some α-pyrones was also investigated in solution and in solid state (table 3), these derivatives showing good emissions in solid state and very weak emissions in CH_2Cl_2. The quantum yields calculated relative to quinine sulfate are very low < 0.1% for isomers **4**, whereas regioisomers **5** exhibit a better emission and their fluorescence quantum yields are slightly higher than that of derivatives **4,** reaching 0.3–0.5 % (table 3).

Table 3. Emission data for α-pyrone derivatives **4** and **5**

	4				**5**			
	Absorption	**Emission**		**Φ_{FL} (%)[c]**	**Absorption**	**Emission**		**Φ_{FL} (%)[c]**
	λ_{max} [nm][a]	**λ_{max} [nm][a]**	**λ_{max} [nm][b]**		**λ_{max} [nm][a]**	**λ_{max} [nm][a]**	**λ_{max} [nm][b]**	
a					367	460	468	0.3
b					373	464	505	0.4
c					382	472	490	0.4
d					370	462	484	0.4
e	368	462	484	0.08	372	463	-	0.4
f	368	462	502	0.05	372	464	478	0.5
g	368	449	470	0.03	371	461	479	0.5
h					366	460	495	0.5

i		368	460	490	0.5

[a] Recorded in CH_2Cl_2

[b] Recorded in solid state

[c] Determined in CH_2Cl_2 with quinine sulfate as reference (Φ = 54%)

We observed that all pure dihydrocyclopenta[*c*]pyrans are green emitters by irradiation at 365 nm in solid state. Thus, by excitation at 370 nm both regioisomers display emissions maxima in the range 449–472 nm in solution and 468–505 nm in solid state, as seen in table 3; therefore the photoluminescence property is not significantly influenced by the nature and position of substituents.

The single crystal molecular structures of **4b**, **4c**, **4e** and **5f** were obtained by X-Ray diffraction using suitable crystals obtained from chloroform or dichloromethane solutions by slow evaporation of the solvent. For example, a closer inspection of the associations of the molecules in the lattices of **5f**'s layered structures (Figure 8) reveals antiparallel orientations of the molecules, as *head-to-tail* disposition. C-H···π interactions of 3.173 Å (blue dashed line) between a hydrogen of the phenyl group of one molecule and the phenyl unit belonging to the vicinal molecule can be observed in the network. The oxygen from the carbonyl group forms H-bonds (red dashed line) with the hydrogen of the *para*-substituted phenyl ring, C-19–H-19···O-2 having the length 2.547 Å, shorter with 0.173 Å than the sum of the van der Waals radii, in an angle of 150.16°.

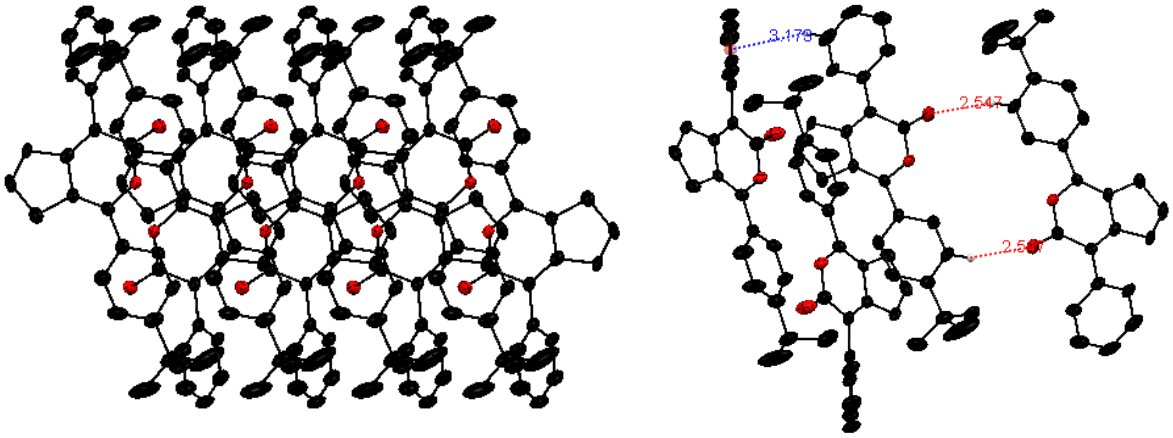

Figure 8. MERCURY representation of the lattice view along *b* axis for compound **5**

1.2.3. Synthesis of aromatic cyclopenta[*c*]pyrans

In order to obtain the aromatic cyclopenta[*c*]pyran derivatives, two synthetic routes, starting from α-pyrones,[10] were taken into consideration:

1. Selective reduction in the presence of DIBAL-H leading to 1,4-disubstituted cyclopenta[*c*]pyrans.

2. Reaction with trimethylaluminum gave the 1,3,4-trisubstituted cyclopenta[*c*]pyrans bearing a methyl group in position 3.

The synthesis of 1,4-disubstitued cyclopenta[*c*]pyran derivatives **6** was carried out in fair yields (12–38%), by selective reduction with DIBAL-H of isomeric mixture of α-pyrone derivatives **4** and **5** (scheme 5). This series of aromatic cyclopenta[*c*]pyrans **6** are deep-red powders that decompose rapidly at room temperature within a few hours, but they can be stored in the freezer for a long period.

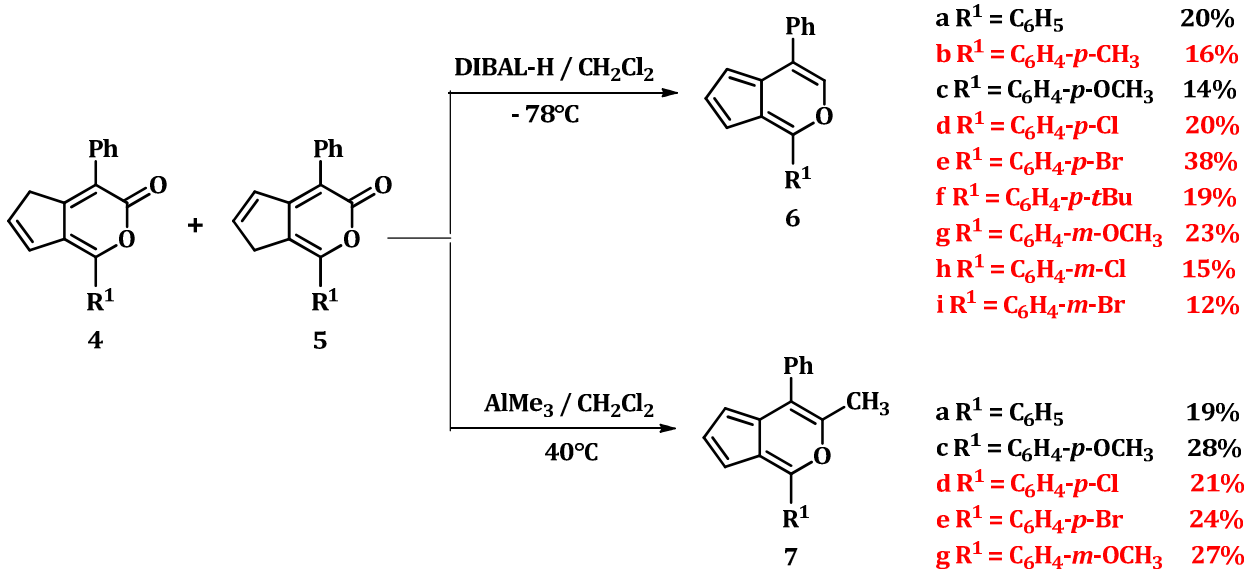

a $R^1 = C_6H_5$	20%
b $R^1 = C_6H_4$-*p*-CH_3	16%
c $R^1 = C_6H_4$-*p*-OCH_3	14%
d $R^1 = C_6H_4$-*p*-Cl	20%
e $R^1 = C_6H_4$-*p*-Br	38%
f $R^1 = C_6H_4$-*p*-*t*Bu	19%
g $R^1 = C_6H_4$-*m*-OCH_3	23%
h $R^1 = C_6H_4$-*m*-Cl	15%
i $R^1 = C_6H_4$-*m*-Br	12%

a $R^1 = C_6H_5$	19%
c $R^1 = C_6H_4$-*p*-OCH_3	28%
d $R^1 = C_6H_4$-*p*-Cl	21%
e $R^1 = C_6H_4$-*p*-Br	24%
g $R^1 = C_6H_4$-*m*-OCH_3	27%

Scheme 5

The 1,4-disubstituted cyclopenta[*c*]pyrans are highly unstable at room temperature. In order to obtain cyclopenta[*c*]pyrans with increased stability, the mixture of α-pyrones **4** and **5** was treated with trimethylaluminum leading to products **7** (scheme 5). After purification by column chromatography on neutral aluminum oxide, five 1,3,4-trisubstituted cyclopenta[*c*]pyrans were obtained in good yields, as deep-red amorphous solids slightly more stable than the corresponding 1,4-disubstituted derivatives **6**. The structure of all derivatives was confirmed by NMR spectroscopy and mass spectrometry.

1.2.4. Electrophilic substitution reactions

The purpose of this research work was the obtaining of fluorescent aromatic cyclopenta[*c*]pyrans. Even if derivatives **6** and **7** fulfilled this requirement, their sensitivity to air, acidic or strong alkaline media represents a real drawback for the potential applications. Therefore, we took into consideration to increase the stability of cyclopenta[*c*]pyran skeleton by introducing electron-withdrawing substituents that would eventually enhance the fluorescence properties. Based on literature data,[2,10] we decided to exploit the aromatic character of cyclopenta[*c*]pyrans towards electrophilic agents. Thus,

the obtained derivatives **6** and **7** were subjected to reactions of trifluoroacetylation and formylation.

Theoretical calculations showed that the electron density is higher at positions 5 and 7, and lower at position 6. Molecular orbital calculations predict the highest electron density at position 7 for the pseudoazulene-[*c*]-series[2].

1.2.4.1. Trifluoroacetylation

The trifluoroacetylation reactions were performed in anhydrous dichloromethane, at room temperature, by reacting the cyclopenta[*c*]pyrans **6** and **7** with trifluoroacetic anhydride in presence of triethylamine, when monosubstituted products **8** and **9**, respectively were obtained (scheme 6).

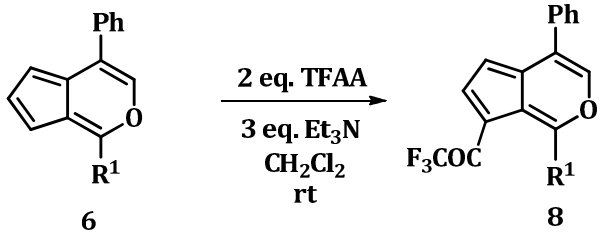

a $R^1 = C_6H_5$	78%
b $R^1 = C_6H_4$-*p*-CH_3	69%
c $R^1 = C_6H_4$-*p*-OCH_3	93%
d $R^1 = C_6H_4$-*p*-Cl	78%
e $R^1 = C_6H_4$-*p*-Br	75%
f $R^1 = C_6H_4$-*p*-*t*Bu	83%
g $R^1 = C_6H_4$-*m*-OCH_3	81%
h $R^1 = C_6H_4$-*m*-Cl	53%
i $R^1 = C_6H_4$-*m*-Br	63%

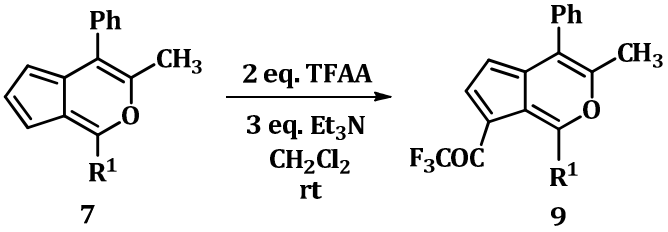

a $R^1 = C_6H_5$	68%
c $R^1 = C_6H_4$-*p*-OCH_3	68%
d $R^1 = C_6H_4$-*p*-Cl	66%
e $R^1 = C_6H_4$-*p*-Br	88%
f $R^1 = C_6H_4$-*p*-*t*Bu	55%
g $R^1 = C_6H_4$-*m*-OCH_3	93%

Scheme 6

As mentioned earlier, the positions susceptible to an electrophilic attack are positions 5 and 7, in which, as stated by theoretical calculations, the electron density is higher[2]. In the case of trifluoroacetylation reaction, only the formation of 7-monosubstituted derivative could be observed, while not even traces of the 5-monosubstituted product were detected. We were able to obtain 13 new trifluoroacetyl-cyclopenta[*c*]pyrans **8** and **9** in very good yields (63% to 93%) using this procedure and their structures were determined by NMR spectroscopy, mass-spectrometry and, in some cases, by X-ray diffractometry as well.

Trifluoroacetylated derivatives **8** and **9** have higher stability compared to the corresponding cyclopenta[*c*]pyrans **6** and **7** and are easy to handle at room temperature.

All trifluoroacetylated derivatives **8** and **9** are deep-red or orange solids that exhibit strong orange fluorescence by irradiation at 365 nm with a UV lamp (figure 9).

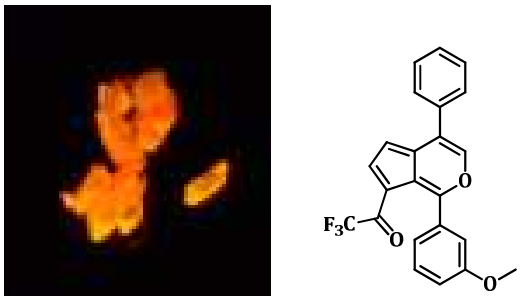

Figure 9. Orange fluorescence of solid compound **8c** by irradiation at 365 nm

Owning two series of cyclopenta[*c*]pyran derivatives possessing the same chromophore, a trifluoroacetyl group in position 7 and a different substituent at position 3 (H or Me) we next investigated their optical properties in solution by UV-Vis absorption and photoluminescence spectroscopy. Figure 10 shows the absorption spectra of derivatives **8** and **9** measured in CH_2Cl_2 at room temperature; their photophysical properties are summarized in table 4.

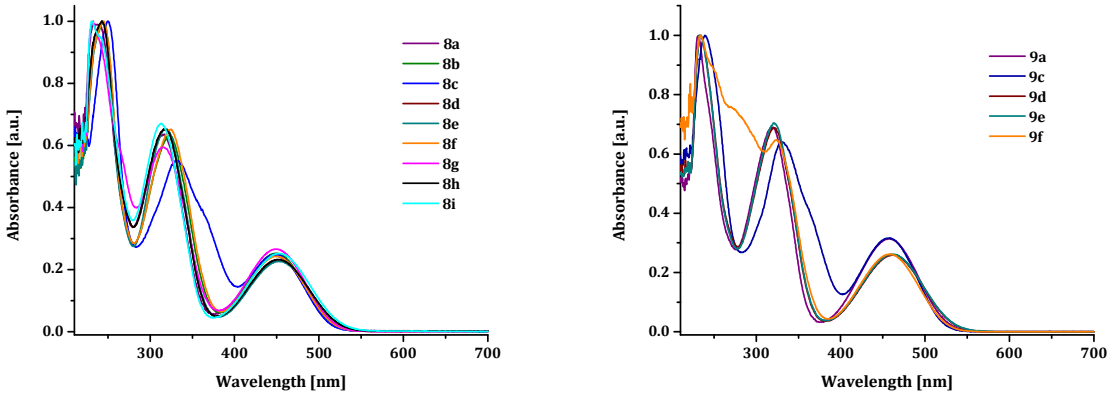

Figure 10. Normalized absorption spectra of derivatives **8** and **9** recorded in CH_2Cl_2

All derivatives display three strong absorption bands in the 230–460 nm range, the higher wavelength (around 450 nm) being ascribed to electronic transitions of CF_3CO group.

Table 4. Absorption and photoluminescence data for trifluoroacetylated-derivatives **8** and **9**

	8				**9**			
	Absorption	**Emission**	***Stokes* shift [cm^{-1}]/(nm)**	**Φ_{FL} (%)[b]**	**Absorption**	**Emission**	***Stokes* shift [cm^{-1}]/(nm)**	**Φ_{FL} (%)[b]**
	λ_{max} [nm][a]	**λ_{max} [nm][a]**			**λ_{max} [nm][a]**	**λ_{max} [nm][a]**		
a	237, 315, ***450***	562	4429 / 112	0.1	230, 318, ***458***	570	4290 / 112	0.09
b	245, 323, ***450***	564	4492 / 114	0.2				
c	245, 333, ***450***	561	4397 / 111	0.3	238, 332, ***458***	563	4072 / 105	0.5
d	242, 318, ***453***	568	4469 / 115	0.05	233, 322, ***463***	572	4116 / 109	0.06
e	242, 318, ***453***	568	4469 / 115	0.05	233, 322, ***463***	576	4237 / 113	0.05
f	243, 323, ***450***	564	4492 / 114	0.1	233, 323, ***458***	567	4197 / 109	0.2
g	233, 315, ***450***	568	4616 / 118	0.07				
h	243, 318, ***450***	567	4586 / 117	0.04				
i	238, 313, ***453***	572	4593 / 119	0.02				

[a] Recorded in CH_2Cl_2

[b] Determined in CH_2Cl_2 with rhodamine 6G as reference (Φ = 96%)

The fluorescent properties of all synthesized compounds were measured in CH_2Cl_2 solutions and are presented in table 4. Derivatives **8** and **9** show yellow–orange fluorescence due to the charge transfer from the electron-donating groups to the accepting trifluoroacetyl group. The photoluminescence wavelengths of the compounds and the Stokes shift are not significantly influenced by the nature of substituents.

The quantum yield of trifluoroacetylated derivatives **8** and **9** was measured using rhodamine 6G (Φ = 0.96) as a standard material. It can be observed (table 4) that compounds **8c** and **9c** have a higher quantum yield than other compounds probably due to the better charge transfer from the *para-methoxy* group to the trifluoroacetyl group.

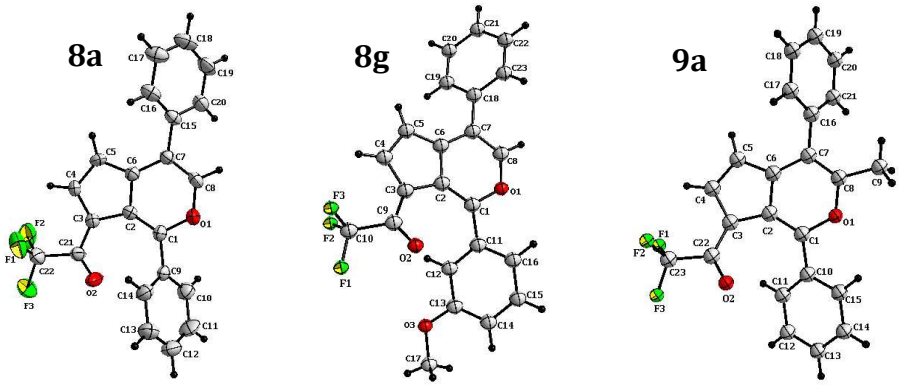

Figure 11. Crystal structures of trifluoroacetyl-cyclopenta[*c*]pyrans **8a**, **8g** and **9a**

The structures of **8a**, **8g** and **9a** (figure 11) were confirmed by X-ray diffraction on monocrystals obtained from $CDCl_3$, by slow evaporation at room temperature.

1.2.4.2. Formylation

The cyclopenta[*c*]pyrans behave differently when are subjected to formylation compared to the trifluoroacetylation reaction. Therefore, depending on the amount of electrophile reagent and reaction time, monosubstituted and/or disubstituted products can be obtained.

Formylation of cyclopenta[*c*]pyrans **6** with two equivalents of $POCl_3$ and excess DMF (having the role of both solvent and reagent) at 45°C over 45 min., led to the formation of a mixture of mono- and disubstituted derivatives, which could not be separated due to the very small polarity differences (scheme 7). Despite these drawbacks, using excess of electrophile reagent (7 eq. $POCl_3$) and increasing the reaction time to 20 hours, we managed to obtain only the disubstituted products **12** in very good yields, which could be thus isolated and characterized.

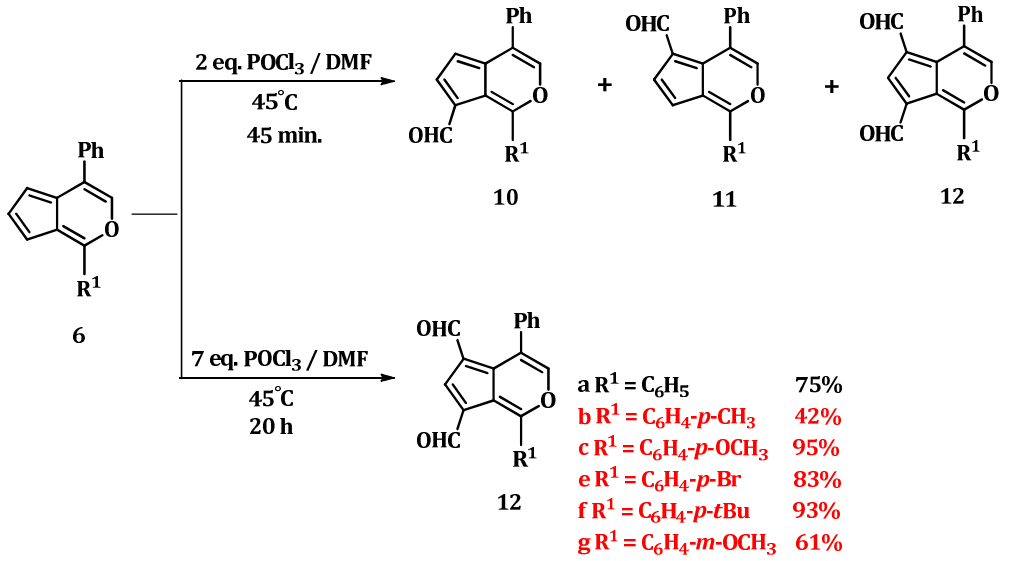

Scheme 7

The absorption and photoluminescence properties of 5,7-diformyl-cyclopenta[*c*]pyrans **12a–g** were studied in CH_2Cl_2 solution at room temperature.

The optical absorption spectra of compounds **12a–g** shown in figure 12 reveal two absorption bands: first absorption band around 293–315 nm is more intense than the second band situated in the 420–428 nm region. The latter can be assigned to an internal charge transfer from the electron donor groups to electron acceptor *CHO*.

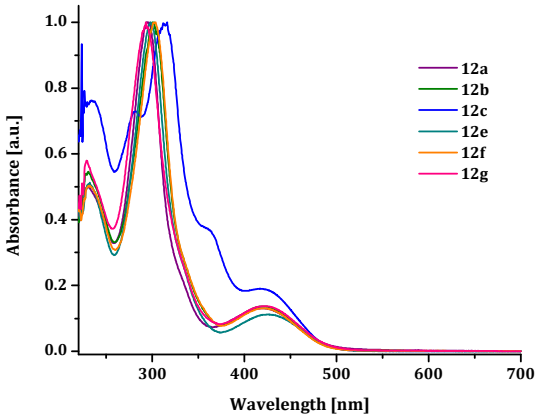

Figure 12. Normalized absorption spectra of derivatives **12** recorded in CH_2Cl_2 at room temperature

Concerning the absorption behavior comparing to reference compound **12a**, a slight bathochromic shift (ca. 3–8 nm) was observed for the derivatives having a phenylene unit decorated with various electron-donating groups (table 5). All the investigated diformyl-cyclopenta[*c*]pyran derivatives are yellow-orange emitters (537–558 nm, table 5).

At a first glance, the emission of the diformylated derivatives looks more promissing than that of trifluoroacetylated-cyclopenta[*c*]pyrans, but the quantum yields calculated relative to rhodamine 123 are again very low (table 5).

Table 5. Absorption and fluorescence data of derivatives **12**

	12			
	Absorption	**Emission**	***Stokes* shift [cm^{-1}]/(nm)**	**Φ_{FL} (%)[b]**
	λ_{max} [nm][a]	**λ_{max} [nm][a]**		
a	295, ***420***	545	5461 / 125	1.4
b	302, ***423***	558	5720 / 135	0.8
c	315, 364 (sh), ***427***	557	5466 / 130	1.3
e	297, ***428***	537	4743 / 109	2.4
f	302, ***423***	556	5655 / 133	0.8
g	293, ***423***	552	5525/ 129	0.9

[a] Recorded in CH_2Cl_2

[b] Determined in CH_2Cl_2 with rhodamine 123 as reference (Φ = 90%)

1.2.5. Synthesis of cyclopenta[*c*]pyrans-based push-pull chromophores

In our continuing interest in the manipulation of the electronic properties of compounds containing cyclopenta[*c*]pyran moiety, we synthesized three molecular donor

(D)–acceptor (A) systems via a Knoevenagel condensation of aldehydes **12** with malonodinitrile in presence of aluminum oxide as base (scheme 8). Derivatives **13** were obtained in good yields ranging from 58 to 91% and their photophysical and electrochemical properties were investigated.

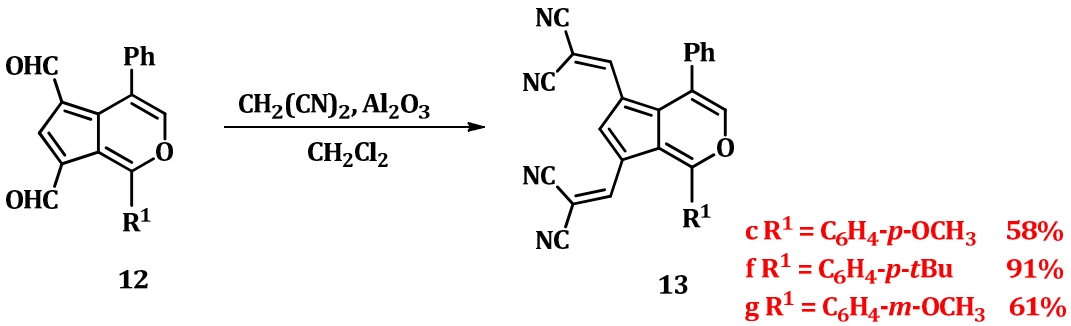

Scheme 8

Figure 13 shows the UV-Vis absorption spectra of compounds **13c**, **f**, **g** in dichloromethane solutions and those of thin film spin-cast on glass from chloroform solutions. The broad maximum wavelength absorption around 450 nm appears to correspond to an intramolecular charge transfer (ICT) between electron-donating and electron-accepting groups, while the absorption band around 360 nm is most likely to be due to π–π* transitions.

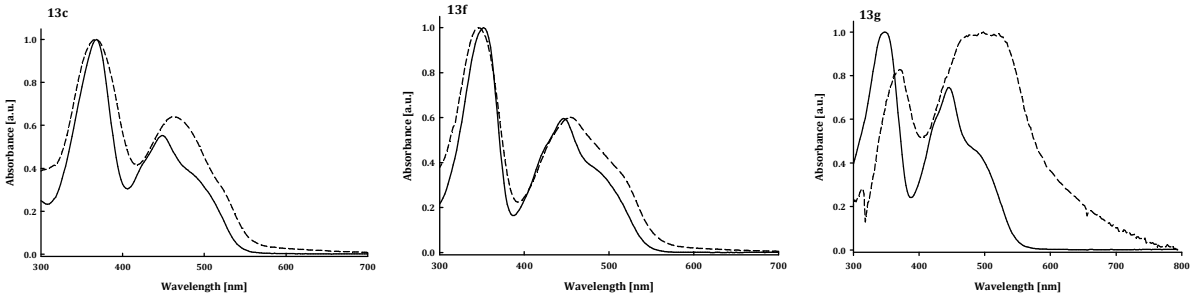

Figure 13. UV-Vis absorption spectra of compounds **13c, f, g**. Solid line: in CH_2Cl_2. Dashed line: as thin film spin-cast on glass from chloroform solutions

As generally observed for π-conjugated systems, the spectra of the films present a red shift of λ_{max} and a broadening of the absorption band reflecting intermolecular interactions in the solid state. Further comparison of the solution and solid-state spectra shows that the smallest difference between the two states is observed for compound **13f** and the largest one for compound **13g**, suggesting differences in intermolecular interactions (table 10).

The intercept of the tangent to the long wavelength absorption edge regarding the spectra of the films with the horizontal axis gave estimated band gaps (E_g) of 2.22 eV for

13f and 2.09 eV for derivative **13g**. These results confirm that, despite limited effects at the molecular level, the nature and position of the substituent on phenylene unit can significantly affect the molecular packing in the solid state.

Table 6. Data of UV-Vis absorption spectroscopy and cyclic voltammetry (0.1 M Bu_4NPF_6/CH_2Cl_2, Pt electrodes, ref SCE) for derivatives **13c**, **f**, **g**

Cmpd.	λ_{max}[a] [nm]	ε_{max}[$M^{-1}cm^{-1}$]	λ_{max}[b][nm]	E_{pa}^1, E_{pa}^2 [V]	E_{pc}^1, E_{pc}^2 [V]	E_g [eV]
13c	450	23990	467	1.60, 1.99	-1.02, -1.11	2.19
13f	446	24865	456	1.62, 1.94	-1.02, -1.11	2.22
13g	445	22482	502	1.62, 1.94	-0.99, -1.5	2.09

[a] In CH_2Cl_2.
[b] Thin films spun-cast on glass.

The cyclic voltammograms of derivatives **13c**, **f**, **g** are similar, showing two irreversible oxidation waves with the first anodic peak potential E_{pa}^1 around 1.60 eV and the second E_{pa}^2 around 1.95 eV (table 6). In the negative region, the CV of all compounds exhibits two irreversible reduction waves indicating the formation of unstable anion radicals. Considering the fact that the open-circuit voltage (V_{oc}) of OPV cells depends on the difference between the LUMO of the acceptor and the HOMO of the donor[13], this high optical gap appears uninteresting and derivatives **13** have not been tested as donors in OPV cells.

1.3. Conclusions

In the first chapter of the thesis, a literature survey with respect to pseudoazulenic heterocyclic system consisting of cyclopenta[*c*]pyran with aromatic skeleton as well as the original results regarding the synthesis of new cyclopenta[*c*]pyran derivatives were presented.

By following a multi-step strategy which starts from 1,3,4-oxadiazin-6-ones, we synthesized six series of cyclopenta[*c*]pyrans: 8 new enol-lactone derivatives, 7 new α-pyrones, 10 new aromatic cyclopenta[*c*]pyrans, 13 new trifluoroacetyl derivatives, 5 new diformyl-cyclopenta[*c*]pyrans and 3 donor-acceptor systems.

The structural analysis of the new compounds was based on complex investigations such as 1D and 2D NMR, UV-Vis/fluorescence spectroscopy, mass spectrometry and X-Ray diffractometry.

Tetra- (**2**) and dihydrocyclopenta[*c*]pyrans (**4** and **5**) were investigated by photophysical and electrochemical analysis. Both series, enol-lactones (**2**) and α-pyrones (**4** and **5**) show strong blue and green fluorescence, respectively, in solid-state by

[13] C. J. Brabec, A. Cravino, D. Meissner, N. S. Sariciftici, T. Fromhertz, M. Rispens, L. Sanchez, J. C. Hummelen, *Adv. Funct. Mater.* **2001**, *11*, 374.

irradiation at 365 nm and weaker emissions in dichloromethane solutions. A general comparison of fluorescence in solid-state and in solution revealed a slight bathochromic shift of emission maxima, probably due to intermolecular interactions in solid-state.

It was observed that the aromatic cyclopenta[*c*]pyrans **6** and **7** do not exhibit fluorescence neither in solution nor in solid-state. However, by introducing electron-withdrawing groups like trifluoroacetyl or formyl, the cyclopenta[*c*]pyran derivatives **8**, **9** and **12** become fluorescent. Furthermore, the electron-withdrawing groups stabilize the cyclopenta[*c*]pyran unit.

X-Ray diffraction of some derivatives showed strong intra- and intermolecular interactions such as H-bonding (C-H···O), C-H···π, C-X···X and C-H···X contacts.

In our attempts to obtain push-pull chromophores with a low band gap, we synthesized three donor-acceptor systems based on cyclopenta[*c*]pyran but these derivatives proved to be unsuitable for optoelectronic devices due to their high optical gap.

Future work will focus on the study of fluorescence quantum yield in solid state for all series of cyclopenta[*c*]pyran derivatives.

Chapter 2: Synthesis and Structural Analysis of new Indenopyrone derivatives

2.1. Introduction

Dihydroindenopyrones are heterocyclic compounds consisting structurally of an indene unit fused to the *c*-bond of a pyrone unit. Functionalized oxygen-containing heterocycles play a proeminent role in medicinal chemistry and in this context, indenopyran derivatives are ''privileged medicinal scaffolds'' which are used for the development of pharmaceutical agents with various applications[14]. Indenopyrans represent a new class of derivatives used as intermediates for the development of Top I anticancer agents such as indenoisoquinoline products.

The important biological functions in nature and the synthetic potential of α-pyrones for the construction of a variety of arenes and heteroarenes challenged us to obtain and investigate new indenopyrone derivatives.

Herein we report the synthesis and study of optoelectronic properties of some substituted indenopyran compounds.

[14] (a) A. V. Karnik, A. M. Kulkarni, N. J. Malviya, B. R. Mourya, B. L. Jadhav, *Eur. J. Med. Chem.* **2008**, *43*, 2615; (b) J. P. Suryavanshi, N. R. Pai Indian, *J. Chem., Sect. B* **2006**, *45*, 1227; (c) T.-S. Jin, J.-S. Zhang, L.-B. Liu, A.-Q. Wang, T.-S. Li, *Synth. Commun.* **2006**, *36*, 2009.

2.2. Original Contributions

Taking into account the potential of the diazalactones to participate as dienophile components in *inverse-electron demand* Diels-Alder reactions, a series of new tetrahydroindeno[*1,2-c*]pyran derivatives was synthesized. Addition of freshly distilled indene (as diene component) to oxadiazinones **1** (dienophile) occurs under acidic conditions, in presence of TFA and TFAA, leading to the formation of tetrahydroindeno*[*1,2-*c]*pyran-3-ones as a mixture of regioisomers (scheme 1).

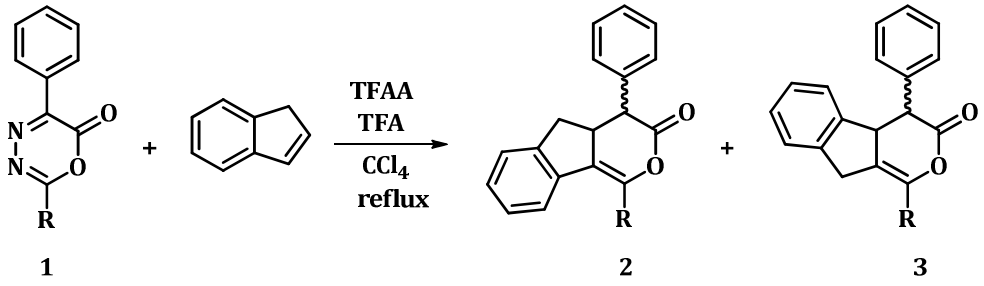

a R = C_6H_5 20 %
b R = C_6H_4-*p*-Br 54 %
c R = C_6H_4-*p*-^{t}Bu 45 %
d R= C_6H_4-*m*-OCH_3 35 %

Scheme 1

The TLC monitoring of the reaction and the NMR spectra revealed the formation of several products; therefore, the cycloaddition proceeds neither stereoselectively, nor regioselectively. In theory, two regioisomers can be formed: isomer **2,** which exhibits the benzen ring condenced at C-*5a*–C-*9a* and its regioisomer **3** having the benzen ring at C-*4b*–C-*8a*. Due to the asymmetric centers found in positions 4 and 4a, each regioisomer can be expressed as a set of diastereoisomers (**2'/3'** possessing the two hydrogen atoms at positions 4 and 4a in a *trans* configuration and **2''/3''** having the two hydrogen atoms in a *cis* configuration, chart 1).

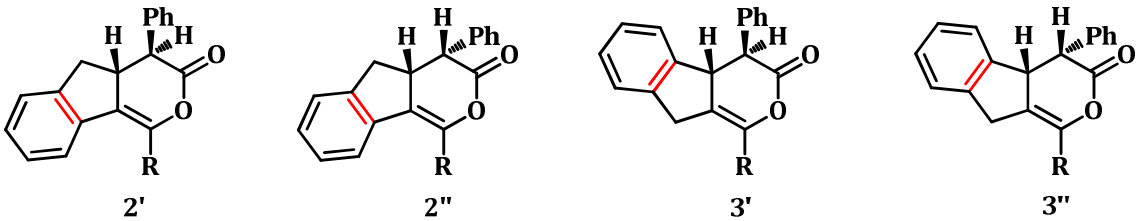

Chart 1.Possible isomers of 3,4,4a,5-tetrahydroindeno*[*1,2-*c]*pyran-3-one **2** and 3,4,4a,9-tetrahydroindeno*[*1,2-*c]*pyran-3-one **3**

In most cases regioisomer **2** is preponderantly formed, on occasion the formation of derivative **3** is not even observed (*e.g.* **3d** derivative) and the nature of the substituent influences the ratio between regio- and diastereoisomers (table 1).

Table 1. Ratios of regio- and diastereoisomers **2** and **3.**
Conditions:
TFAA 1.5 eq.; TFA 1.55 eq.; indene 6 eq.; 9 days reflux, CCl_4

	Ratio			
	2'	**2''**	**3'**	**3''**
a R = C_6H_5	1	-	-	0.2
b R = C_6H_4-*p*-Br	1	1	-	0.25
c R = C_6H_4-*p*-^{t}Bu	1	1	0.2	-
d R = C_6H_4-*m*-OCH_3	1.2	1	-	-

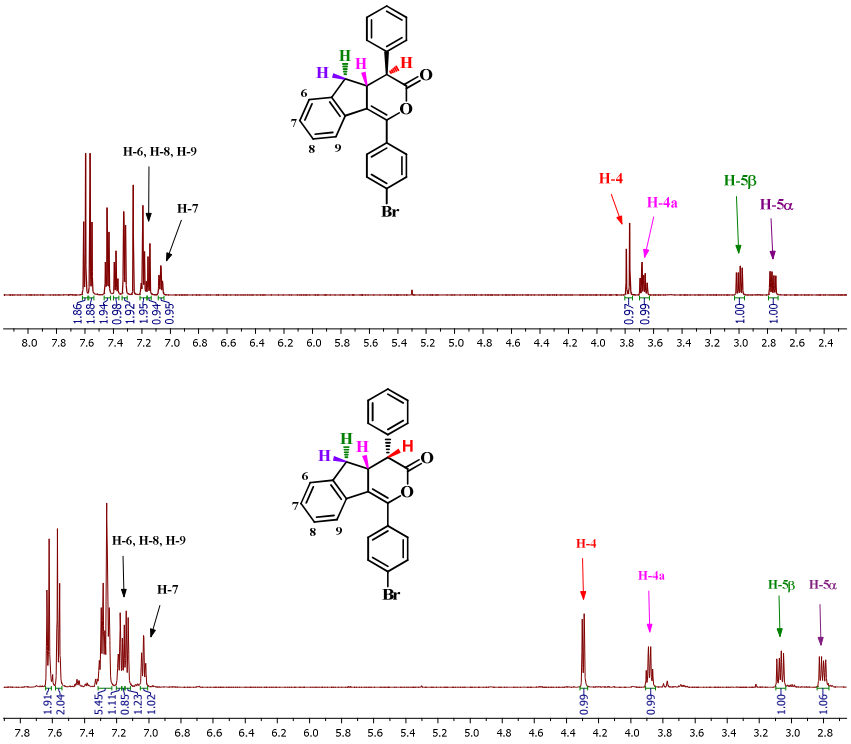

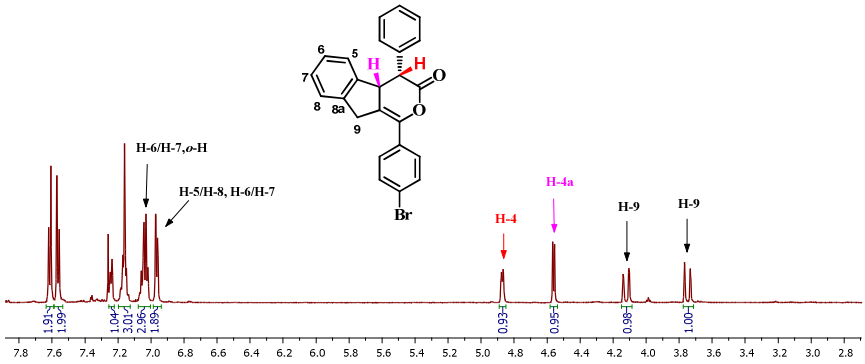

Figure 1. ^{1}H NMR spectra (600 MHz, $CDCl_3$) of isomers **2'b** (top), **2''b** (middle) and **3''b** (bottom)

The configuration of the diastereoisomers was assigned by ^{1}H NMR spectroscopy. Analyzing the ^{1}H NMR spectra (figure 1) of isomers **2'b**, **2''b** and **3''b** significant differences are observed, especially for the hydrogen atom of the stereocenter C-4. For isomer **2'b** the large coupling constant ($J_{4,4a}$ = 14.3 Hz) indicates the *trans* orientation of H-4 relative to H-4a, while the proton H-4 in isomer **2''b** exhibits a more deshielded doublet with a moderate coupling constant ($J_{4,4a}$ = 7.1 Hz) characteristic for the *cis* configuration. On the other hand, the ^{1}H NMR spectrum confirmed the formation of *cis* diastereoisomer **3''b** ($J_{4,4a}$ = 6.7 Hz). In case of isomer **3''b** the specific protons of the enol-lactone moiety appear more deshielded than those of isomer **2''b** (figure 1).

With various 1,4-disubstituted indenopyrone derivatives in hand, we next investigated their photophysical properties, the absorption spectra of indeno-derivatives measured in acetonitrile and dichloromethane being shown in figures **2** and **3**. Absorption spectra suggest little differences in the electronic band structures for **2a-d** in acetonitrile and dichloromethane, respectively. Intense broad absorption bands are present in areas ranging from 275-282 nm and 307-317 nm, respectively, values typical for π - π* and n - π* transitions.

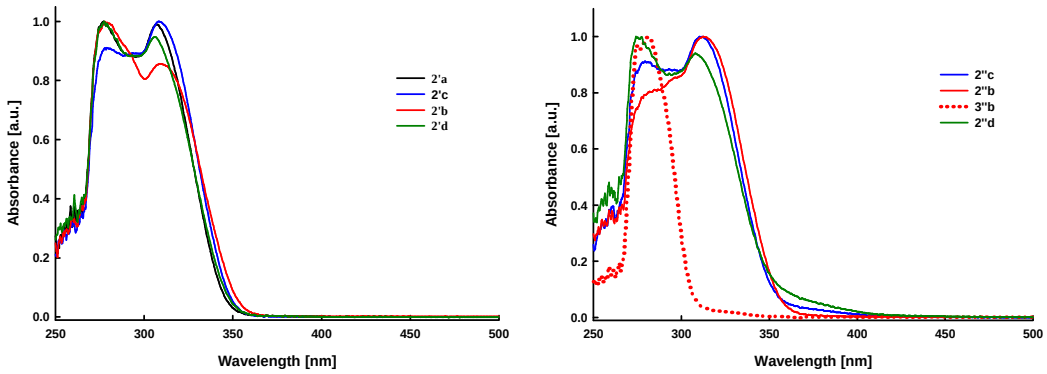

Figure 2. Normalized absorption spectra of dihydroindenopyrones **2'** (left) and **2''** (right) in acetonitrile (298 K)

The analysis of the absorption spectra (figure 3) revealed some differences between diastereoisomers **2'** and **2''**, as well as between regioisomers **2''b** and **3''b**. For example, if we compare the *trans* isomers **2'** with the corresponding *cis* isomers **2''** a small shift to higher wavelength can be observed. A notable red effect (35 nm) is also observed when the regioisomer **2''b** (λ_{max} = 317 nm) and the corresponding derivative **3''b** (λ_{max} = 282 nm) are compared. This behavior could be explained by the enhancement of electron delocalization in the conjugated system in the case of derivative **2''b**.

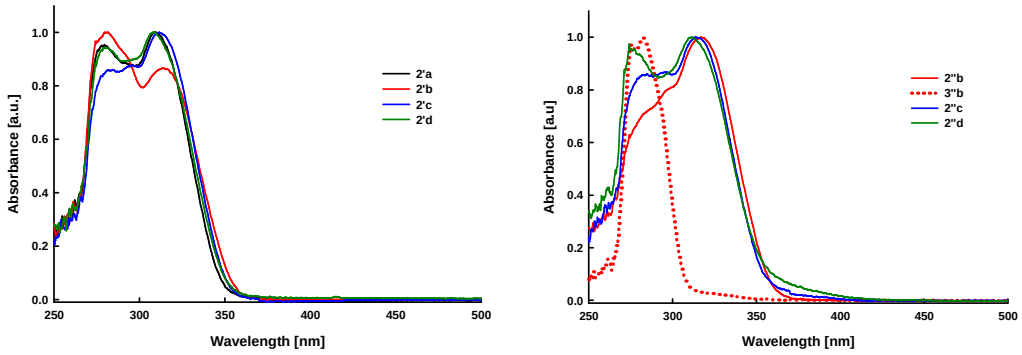

Figure 3. Normalized absorption spectra of diastereoisomers **2'** (left) and **2''** (right) in dichloromethane (298 K)

The fluorescence properties of the indeno-pyrone derivatives were also investigated; details about the emission maxima and quantum yield are shown in table 2.

Table 2. Absorption and emission data for dihydro-indenopyrone derivatives

Compound	Absorption λ_{max} [nm][a]	Emission λ_{max} [nm][a]	Emission λ_{max} [nm][b]	Stokes shift [nm][a]	Φ[c]
2'a	307	382	423	75	7.2 %
2'b	310	389	445	79	18.1 %
2''b	313	393	432	80	5.4 %
3''b	282	392	-	110	0.3 %
2'c	308	384	-	76	12.6 %
2''c	312	338; 354; 370	475	58	7.2 %
2'd	307	386	461	79	10.8 %
2''d	309	391	491	88	3.6 %

[a] Recorded in acetonitrile. [b] In solid state. [c] Determined in acetonitrile with 9,10-diphenylanthracene as reference (Φ = 90%)[15]

The maximum emission bands of compounds **2a-d** are located at about 370–393 nm, suggesting that all investigated indeno-derivatives are blue emitters. Remarkably, the

[15] A. M. Brouwer, *Pure Appl. Chem.* **2011**, 83, *12*, 2213.

fluorescence quantum yield calculated relative to 9,10-diphenylanthracene is significantly higher in case of *trans* isomers **2'** as compared to the corresponding *cis* isomers **2''** (table 2). The photoluminescence properties of some dihydroindenopyrones were also investigated in solid state, these derivatives showing emissions maxima in the range of 423–491 nm when excited at 310 nm (table 2).

In 1998, Christl et al.[16] reported indeno-α-pyrone derivatives prepared in a one-pot procedure starting from 6*H*-1,3,4-oxadiazin-6-ones.

A procedure described in the literature[10] for the oxidation of 3,4,4a,5-tetrahydrocyclopenta[*c*]pyran-3-ones in presence of DDQ was adapted for the synthesis of α-pyrones **4**, **6** and **6'** (schemes 2 and 3). The enol-lactone isomeric mixture was subjected to dehydrogenation and three α-pyrones (**4**, **6** and **6'**) were obtained in rather low yields.

Dehydrogenation of the isomeric mixture **2'a/3''a** was carried out in toluene at 80°C for 6 days in presence of DDQ (scheme 2). Investigations carried out after the purification of crude product showed that isomer **3''a** was fully oxidized to derivative **4** (15% yield). Meanwhile, isomer **2'a** was recovered almost unreacted and only traces of partially oxidized derivative **5** were detected in the NMR spectrum.

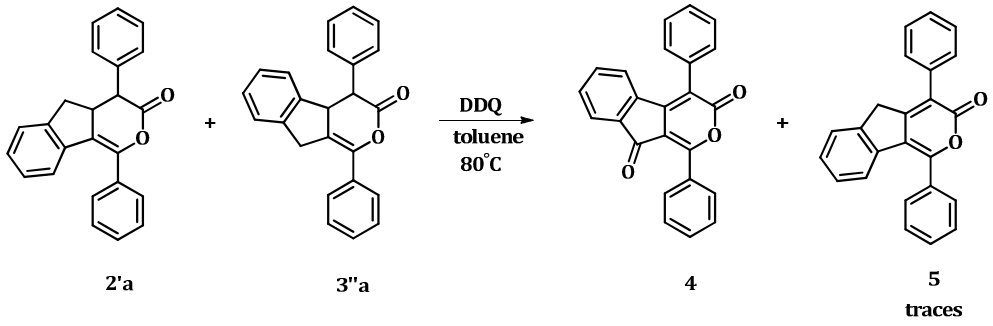

Scheme 2

Using the same procedure, the enol-lactone isomeric mixture **2'c/3'c** was subjected to dehydrogenation and in this case a mixture of regioisomers, namely **6** and **6'** was obtained in 17% yield (scheme 3). The ^{1}H NMR spectrum revealed the formation of fully oxidized derivative **7** in a very small amount, which could not be isolated. After purification by column chromatography on silica gel, the starting enol-lactone derivative **2'c** was recovered in 50% yield.

[16] T. T. Tidwell, F. Sammtleben, M. Christl, *J. Chem. Soc., Perkin Trans. 1* **1998**, 2031.

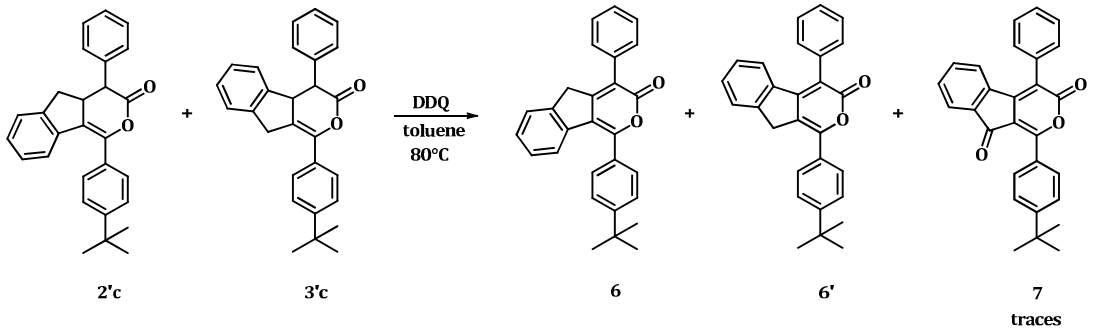

Scheme 3

The optoelectronic and photoluminescence properties of the obtained compounds were also investigated, all spectra being recorded in methylene chloride. The UV-Vis absorption spectra (figure 4) show for all three compounds two absorption maxima at around 275 nm and 370 nm, respectively which could be assigned to the π–π* and n–π* transitions. A bathochromic shift (10 nm) in the absorption spectra due to the extended conjugation can be seen in the case of derivative **6'** as compared to its regioisomer **6**. All derivatives show very weak emissions in the range 380–550 nm (figure 4) when excited at 370 nm and the quantum yields calculated relative to 9,10-diphenylanthracene were extremely low (<1%).

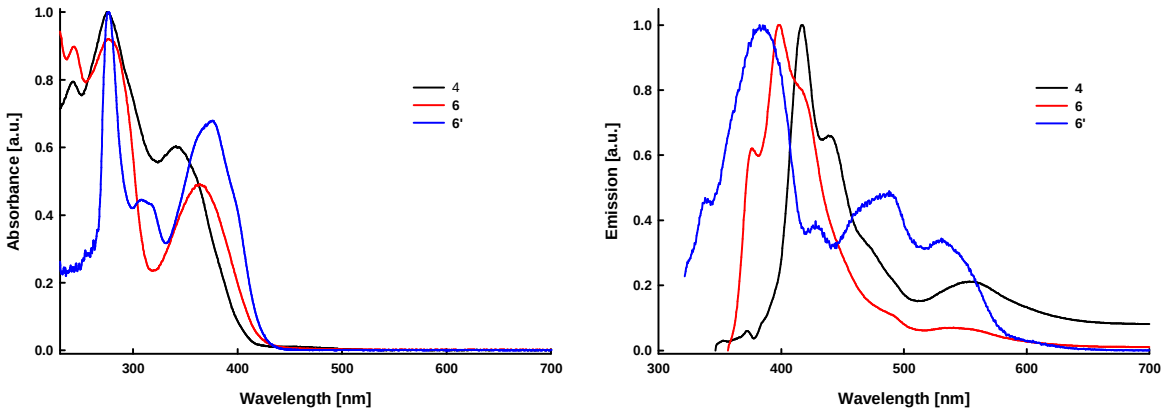

Figure 4. Normalized absorption (left) and fluorescence (right) spectra of α-pyrone derivatives **4**, **6** and **6'** in dichloromethane

2.3. Conclusions

New indenopyrone derivatives have been synthesized and fully analyzed by NMR, UV-Vis and fluorescence spectroscopy, mass spectrometry and X-Ray diffractometry.

Separation of diastereoisomers was possible in a small amount in all cases.

All synthesized derivatives are blue emitters, the indenopyrones having a weaker emission than the corresponding dihydroindenopyrone derivatives.

It was observed that the fluorescence quantum yield calculated relative to 9,10-diphenylanthracene is significantly higher for the *trans* isomers as compared to the corresponding *cis* isomers.

A general comparison of fluorescence spectra in solution and in solid state revealed an important red shift of λ_{max} and a broadening of the emission band due to intermolecular interactions in solid state.

Chapter 3: Design, Synthesis and Structural Analysis of some Molecular Architectures based on Cyclopenta[*c*]pyrans as Potential Logic Gates

3.1. Introduction

Due to the increasing demands of miniaturization in informatics technology (IT), chemistry plays a key role through the development of supramolecular systems that can behave similar to semiconductors and could be used for the construction of computers (memories, logical gates)[17]. For the implementation of these functions, molecular and supramolecular systems must be able to respond to some chemical and/or physical stimuli (**input**: complexations, pH modifications, redox or other chemical reactions, irradiation at different wavelengths, etc.) and generate one or more response signals (**output**: fluorescence, changes in electrochemical properties etc.). Recently, important progress was made in developing molecular logic gates which use the fluorescence property as **output**, in most cases the fluorescence property being induced by pH modification, complexation with metal ions or by irradiation.[18,19,20,21,22,23,24,25,26,27]

---

[17] (a) A. P. de Silva, N. D. McClenaghan and C. P. McCoy, *Molecular-Level Electronics, Imaging and Information, Energy and Environment, in Electron Transfer in Chemistry*, Wiley-VCH **2001**, Vol. 5; (b) V. Balzani, A. Credi, M. Venturi, *Molecular Devices and Machines – A Journey into the Nanoworld*, Wiley-VCH, **2003,** 235; (c) A. P. de Silva, N.D.McClenaghan, *Chem. Eur. J.*, **2004**, *10*, 574; (d) F. M. Raymo, *Adv. Mater*. **2002**, *14*, 401; (e) G. J. Brown, A. P. de Silva, S. Pagliari, *Chem. Commun*. **2002**, *21*, 2461.

[18] A. P. de Silva, N.D. McClenagh, *Chem. Eur. J.* **2004**, *10*, 574.

[19] U. Pischel, *Angew. Chem.Int. Ed.* **2007**, *46*, 4026.

[20] G. Zong, L. Xian, G. Lu, *Tetrahedron Lett.* **2007**, *48*, 3891.

[21] H. N. Lee, N. J. Singh, S. K. Kim, J. Y. Kwon, Y. Y. Kim, K. S. Kim, J. Yoon, *Tetrahedron Lett.* **2007**, *48*, 169.

[22] H. Okamoto, M. Kohno, K. Satake, M. Kimura, *Bull. Chem. Soc. Japan* **2005**, *78*, 2180.

[23] G. McSkimming, J. H. R. Tucker, H. Bouas-Laurent, J.P. Desvergne, *Angew. Chem.Int. Ed.* **2000**, *39*, 2167.

[24] C.-J.Fang, Z. Zhu, W. Sun, C.-H. Xu, C.-H.Yan, *New J. Chem.* **2007**, *31*, 580.

3.2. Original Contributions

The aim of this chapter is to outline the design and synthesis of molecular assemblies based on modified cyclopenta[*c*]pyran units able to mimic a logic gate. These systems should be structurally modified by the influence of a chemical or electrochemical stimulus in order to work as potential devices for molecular electronics. Figure 1 outlines the minimum required condition to obtain a **logic gate.** The molecular system must be reversibly interconverted between at least two stable states by use of an external stimulus. In the two states, these compounds must exhibit different values of at least one property, which is considered to be the answer.

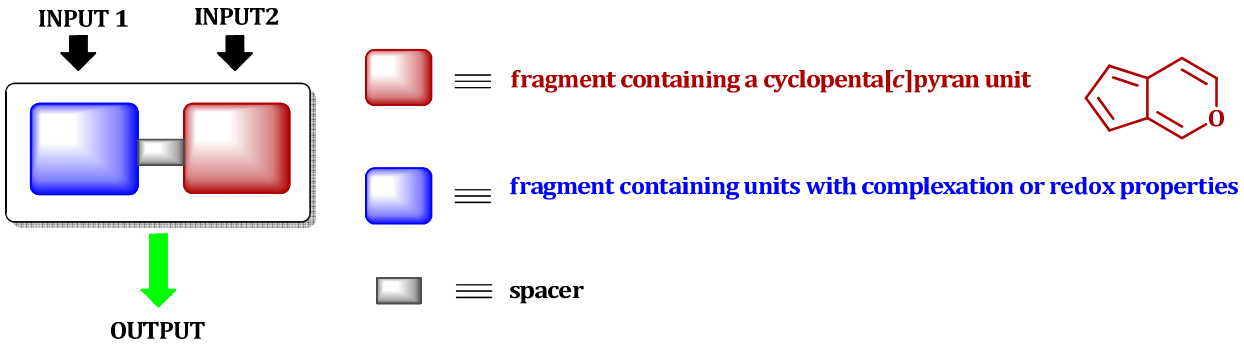

Figure 1

The target compounds contain a cyclopenta[*c*]pyran unit linked through a spacer to a fragment of terpyridine or phenothiazine that is able to undergo a reversible complexation–decomplexation or a redox reaction, respectively. External stimuli, in our case a complexation–decomplexation or a redox process, determine the interconversion of the molecule between at least two stable states. These stimuli will be used as **INPUT 1** and **INPUT 2** (which is **1** when the signal is positive or **0** if the signal is missing). Depending on the combination of the two signals (**input 1** and **input 2**), the molecule exhibits or not fluorescence, which determines the answer = **OUTPUT** (which is **1** when the molecule exhibits fluorescence and **0** when the fluorescence is absent).

Taking into account the requirements for the design of a logic gate we synthesized two series of derivatives, type **3** (scheme 2) and **5** (scheme 3), one of them containing a terpyridine unit (because of the complexation properties of these units) and another containing a phenothiazine moiety (for its redox properties).

---

[25] S. Uchiyama, G. McClean, K. Iwai, A. P. de Silva, *J. Am. Chem. Soc.* **2005**, *127*, 8920.
[26] Y. Shiraishi, Y. Tokitoh,T. Hirai, *Chem.Comm.* **2005**, *42*, 5316.
[27] D.C. Magri, G. D. Coen, R.L. Boyd, A. P. de Silva, *Anal. Chim. Acta* **2006**, *568*, 156.

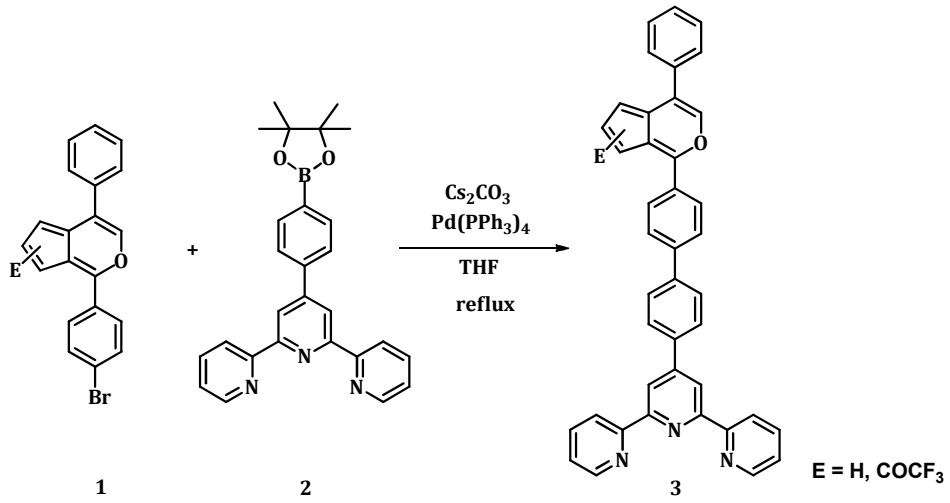

Cmpd.	E	Yield (%)
3a	H	69
3b	$COCF_3$	43

Scheme 2

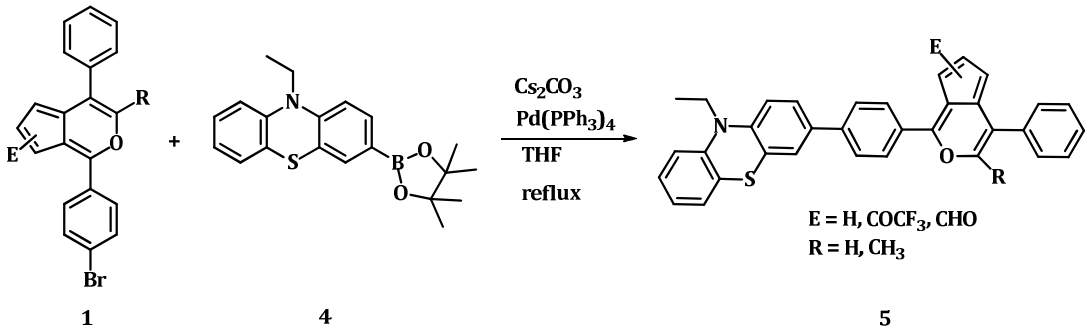

Cmpd.	E	R	Yield (%)
5a	H	H	54
5b	CHO	H	53
5c	$COCF_3$	CH_3	56

Scheme 3

The absorption and photoluminescence properties of all derivatives were also investigated and table 1 summarizes their photophysical data.

Table 1. Absorption and emission data of derivatives **3a-b**, **5a-c**

Compound	Absorption λ_{max} [nm][a]	Emission λ_{max} [nm][a]	Stokes shift [cm^{-1}]
3a	333	390	4389
3b	455	570	4482
5a	375	473; 530 (sh)	5525
5b	400	550	6818
5c	425	570	5985

[a] Recorded in dichloromethane at room temperature.

Regarding the fluorescence properties, some of compounds have emissions in the blue-green region (**3a**, **5a**) and others in the yellow-orange one (**3b**, **5b**-**c**, table 1). Derivatives **5a**-**c**, containing a phenothiazine unit, exhibit weaker emissions than those with terpyridine structure (**3a**-**b**). Furthermore, the emission band maximum is significantly red shifted (*ca.* 100 nm) for the derivatives bearing an electron-withdrawing group, such as CHO and $COCF_3$.

Next, derivatives **3a**-**b** were tested as potential logic gates. In this context, having molecular systems that contain a guest binding site (terpyridine unit) and a photon interaction site (cyclopenta[*c*]pyran moiety) as components, a photoinduced electron transfer (PET) mechanism between the two sites can switch the luminescence ''on'' by chemical means, such as complexation reactions.

The UV-Vis spectrum of terpyridine-based derivative **3a** displays two absorption maxima below 300 nm, assigned to the π-π∗ electronic transitions in the pyridine rings and an absorption band at 330 nm ascribed to n-π∗ electronic transitions in the cyclopenta[*c*]pyran unit (figure 2, black line). The absorption spectrum recorded in acidic conditions reveals a conformational change in the terpyridine unit from *trans, trans* conformation to the planar *cis, cis* conformation (maximum band at 418 nm, red line). UV-Vis spectrum of the Fe (II) complex shows the characteristic band of the planar *cis*, *cis* conformation and a band at 575 nm assigned to the metal-ligand charge transfer, MLCT (figure 2, green line).

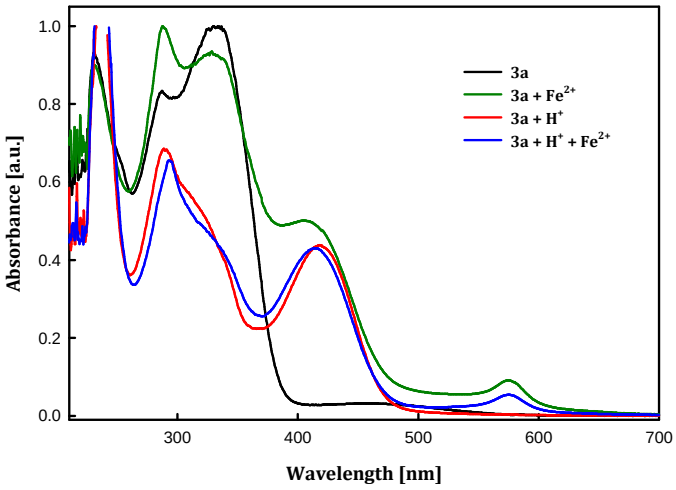

Figure 2. Normalized absorption spectra of derivative **3a** recorded under various conditions (inputs)

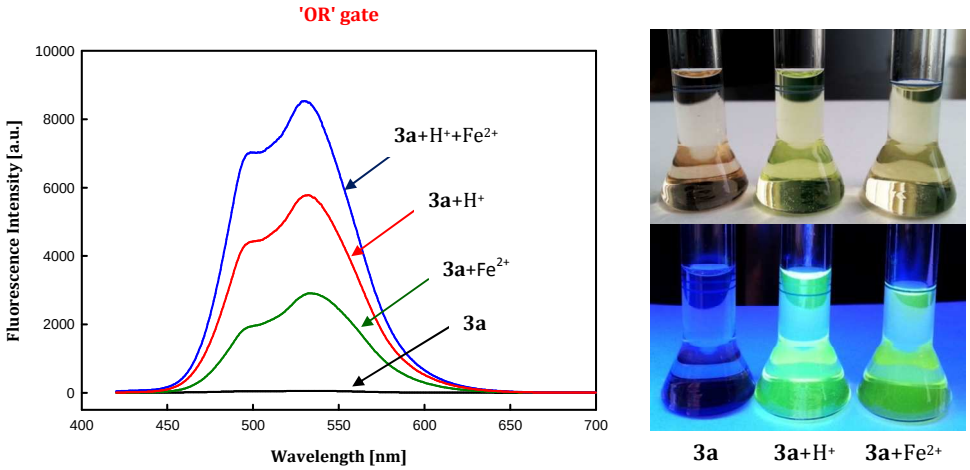

Truth table of derivative **3a**

Input$_1$ **H$^+$**	**Input$_2$** **Fe^{2+}**	**Output** **Luminescence**[a]
Low (0 M)	Low (0 M)	Low (0.08)
Low (0 M)	High (1.3x10^{-2} M)	High (0.27)
High (0.05 M)	Low (0 M)	High (0.56)
High (0.05 M)	High (1.3x10^{-2} M)	High (0.83)

[a]Quantum yields in CH_2Cl_2, reference standard rhodamine 6G (0.96);

λ_{exc} = 400 nm; λ_{em} = 530 nm.

Figure 3. Fluorescence spectra of compound **3a** and the truth table for **OR** logic gate

Classical logic gates have two input ports and one output port. The experiment performed on derivative **3a** has revealed a logic gate. Thus compound **3a,** which operates

with H^+ and Fe^{2+} as inputs while employing ultraviolet light as power supply and green light as the output (figure 3) mimics an 'OR' gate. The system's luminescence is switched ''on'' when the terpyridine receptor binds either of two analytes, H^+ and Fe^{2+}.

Compound **3b,** which has a strong electron-withdrawing group, $COCF_3$, attached to the fluorophore (cyclopenta[*c*]pyran) does not operate as a logic gate (figure 4). This is most likely due to the PET process not being arrested by the arrival of the analyte at the receptor site. The arrest does not occur due to a continuous competition between the trifluoroacetyl group and the ions used for complexation.

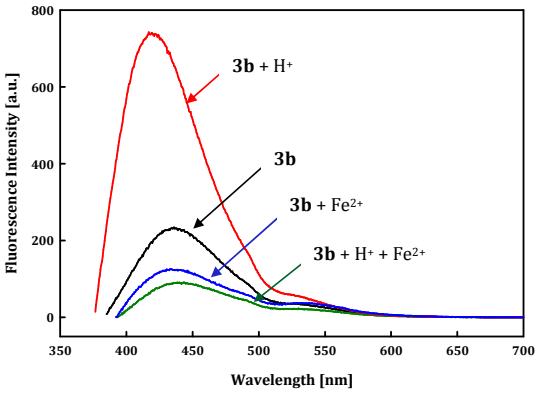

Truth table of derivative **3b**

Input$_1$ H^+	**Input$_2$** Fe^{2+}	**Output Luminescence[a]**
Low (0 M)	Low (0 M)	Low (0.006)
Low (0 M)	High (0.03M)	Low (0.004)
High (0.04 M)	Low (0 M)	Low (0.015)
High (0.04 M)	High (0.03 M)	Low (0.003)

[a]Quantum yields in CH_2Cl_2, reference standard quinine sulphate (0.54); λ_{exc} = 300 nm; λ_{em} = 420 nm.

Figure 4. Fluorescence spectra and truth table of derivative **3b** with various inputs

3.3. Conclusions

Two series of molecular systems based on terpyridine and phenothiazine structures have been synthesized and fully characterized by NMR, UV-Vis, fluorescence spectroscopy and mass spectrometry.

Attempts have been made to determine the possibility to use these systems in molecular electronics as potential logic gates.

We demonstrated that compound **3a** is able to mimic an ''OR'' gate as it shows important differences in the fluorescence intensity when going from uncomplexed to complexed derivative.

Future work will consist on the analysis of derivatives **5a-c** with a focus on their potential as logic gates using this time an electrochemical stimulus as input.

Chapter 4: Small Molecular Donors for Organic Photovoltaics

4.1. Introduction

The design of an OPV cell involves the creation of a heterojunction by interfacing an electron donor material with an electron acceptor material.[28]

Usually, an organic solar cell is composed of five components: a) a support substrate coated with a transparent conductive oxide, ITO; b) a thin layer of poly(3,4-ethylenedioxythiophene):poly(styrenesulphonate) (PEDOT:PSS) as hole injection layer; c) an active layer comprising donor materials; d) a layer containing the acceptor material and e) a metal electrode, such as Al, as the cathode (figure 1).

Almost all organic solar cells (OSC) have a planar-layered structure, where the organic light-absorbing layer is sandwiched between two different electrodes. One of the electrodes must be transparent, often indium tin-oxide (ITO), the other electrode is a metal like aluminum.

Figure 1 illustrates the device structures for bilayer heterojunction (a) and bulk heterojunction (b) as well as the fundamental steps occurring in donor–acceptor heterojunction solar cells (c). There are four steps in converting photons to free charge carriers:

1. Light absorption of donor, leads to exciton formation (an electron is promoted from the highest occupied molecular orbital (HOMO) of donor to its lowest unoccupied molecular orbital (LUMO)).
2. Diffusion of the exciton within the active layer to the donor–acceptor interface.
3. Dissociation of exciton from the LUMO of the donor to the LUMO of the acceptor to create free charge carriers that can reach the electrodes.
4. Collection of free charge carriers at the electrodes (holes at the anode and electrons at the cathode).

[28] C. W. Tang, *Appl. Phys. Lett.* **1986**, *48*, 183.

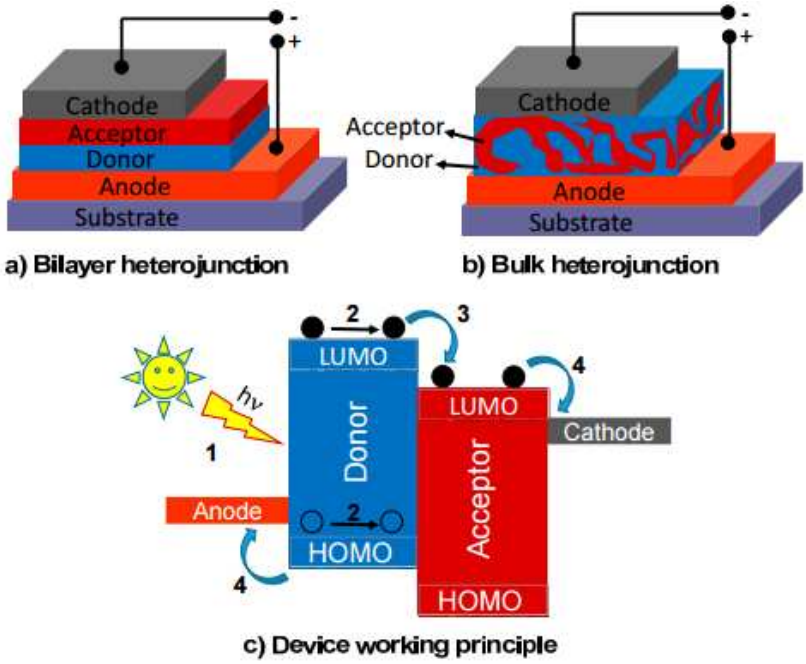

Figure 1. Device structures of (a) bilayer heterojunction; (b) bulk heterojunction; (c) device working principle from light absorption to charge collection

4.2. Original Contributions

The goal of this research is to develop new low band gap small molecular donors for solar cells applications with a focus on:

1. The development of new D-A molecules in which a diphenylhydrazone block is connected to a dicyanovinyl acceptor through π-conjugated spacers;
2. The obtaining of ADDA and ADADA systems based on triphenylamine as molecular donors for organic photovoltaics.

In both cases, the evaluation of their potential as donor materials was done in basic bilayer PHJ cells.

4.2.1. Synthesis and Characterization of new D-A systems

The first objective of my research work developed during my PhD. stage at the University of Angers (MOLTECH–ANJOU) was to obtain new D-A molecules in which a *N*,*N*′-diphenylhydrazone donor unit is linked to a dicyanovinyl acceptor group through π-conjugated spacers based on: thiophene (**1**), bithiophene (**2**), thieno[3,4*b*]thiophene (**3**), 3,4-ethylenedioxythiophene (EDOT, **4**), bis-EDOT (**5**), cyclopentadithiophene (**6**) and dithienopyrrole (**7**, figure 2). These derivatives combine the advantage of a simple, clean

and efficient synthesis with physical properties allowing their implementation into devices using solution and vacuum deposition process.

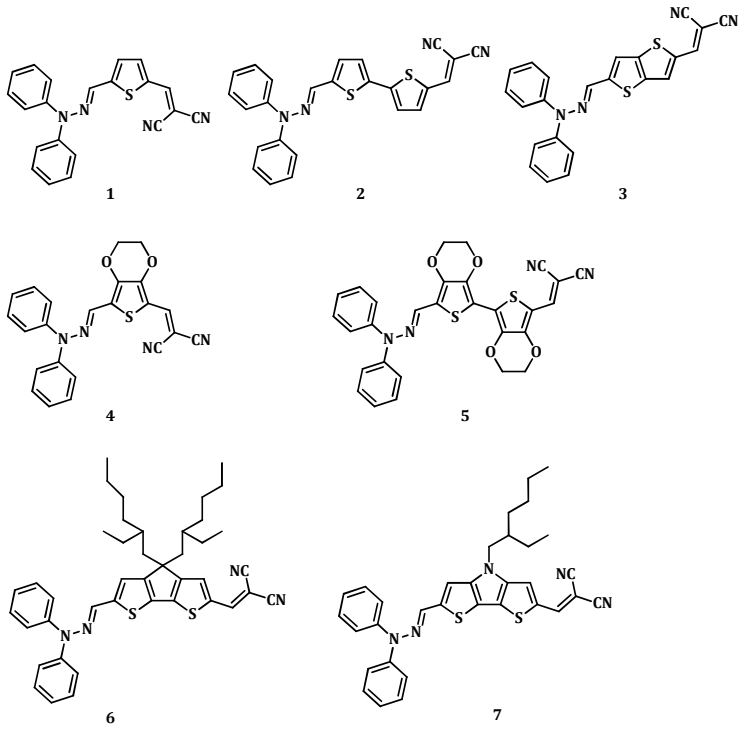

Figure 2. Chemical structures of the target D-A molecules

The synthesis of the target compounds is depicted in scheme 1. Derivatives **1**, **2**, **6** and **7** were synthesized in a similar stepwise synthetic protocol. First, 0.5 equivalent of *N,N'*-diphenylhydrazine **11'** was reacted with one equivalent of the corresponding dicarboxaldehyde derivatives **12'** in THF/CH_3OH in presence of sodium acetate to afford hydrazones **8'a-d** in moderate yields. Under these conditions, aldehyde **8'a** was obtained in 62% yield (based on **11'**) together with 21% of the bis-adduct **13'a** while 18% of the starting dialdehyde **12'a** was recovered.[29] In case of diformylbithiophene **12'b** the formation of aldehyde **8'b** along with bis-adduct **13'b** in 37 and 17% yield, respectively was also observed[30], while for derivatives **12'c** and **12'd** the formation of bis-adduct was not observed. Derivatives **3**, **4** and **5** were obtained using a similar procedure, but in this case starting from the corresponding monoaldehyde derivatives **10'e-g**. Condensation of *N,N'*-diphenylhydrazine **11'** with monoaldehydes of thienothiophene (**10'e**), EDOT (**10'f**) and bis-EDOT (**10'g**) gave compounds **9'e-g** in 51 to 63% yields. In the next step, derivatives **9'e-g** were subjected to a Vilsmeier–Haack formylation in presence of $POCl_3$ and DMF as reagents. Finally, a Knoevenagel condensation of aldehydes **8'a-g** with malonodinitrile in chloroform, in presence of triethylamine as base gave the target

[29]D. Demeter, S. Mohamed, A. Diac, I. Grosu, J. Roncali, *ChemSusChem* **2014**, *7*, 1046.
[30]A. Diac, D. Demeter, M. Allain, I. Grosu, J. Roncali, *Chem. Eur. J.* **2015**, *21*, 1598.

compounds **1**–**7** in 62 to 96% yields. The corresponding mono- and dialdehydes were obtained in good yields, accordingly to known procedures previously described in the literature.[31] All obtained compounds were fully characterized by NMR, UV-Vis spectroscopy, mass spectrometry, cyclic voltammetry and X-Ray diffractometry.

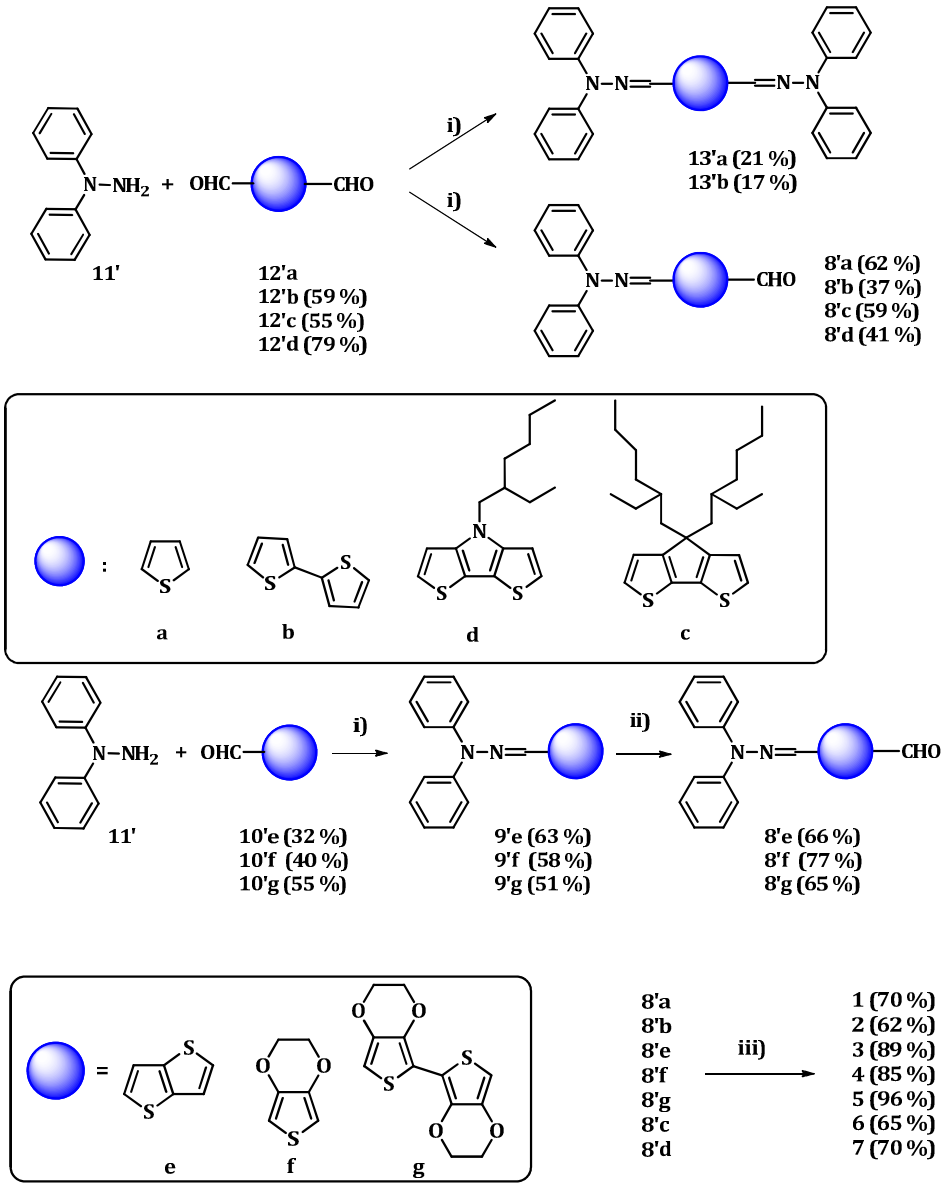

Scheme 1. Synthesis of the target compounds **1-7**. i) AcONa, MeOH/THF; ii) $POCl_3$, DMF, 1,2-dichloroethane; iii) $CH_2(CN)_2$, Et_3N, $CHCl_3$

[31] a) J. Roncali, L. Rasmussen, C. Thobie-Gautier, P. Frère, M. Sallé, H. Brisset, A. Gorgues, M. Jubault, J. Becher, J. Orduna, *Adv. Mater.* **1994**, *6*, 841; b) J.-M. Raimundo, P. Blanchard, N. Gallego-Planas, N. Mercier, I. Ledoux-Rak, R. Hierle, J. Roncali *J. Org. Chem*. **2002**, *67*, 205; c) K.C. Li, Y.C. Hsu, J.T. Lin, C.C. Yang, K.H. Wei, H.C. Lin, *J. Polym. Sci. A*, **2009**, *47*, 2073; d)P. Leriche, J.-M. Raimundo, M. Turbiez, V. Monroche, M. Allain, F.-X. Sauvage, J. Roncali, P. Frère, P. J. Skabara, *J. Mater. Chem.* **2003**, *13*, 1324.

Optical properties

The corresponding data of UV-Vis absorption spectra of compounds **1**–**7** recorded in methylene chloride solutions and as thin films spin-cast on glass are collected in table 1.

Table 1. UV-Vis spectroscopy data ((s): ~1×10^{-5} M in CH_2Cl_2); (f): films spin-cast on glass), and cyclic voltammetry (in 0.10 M Bu_4NPF_6/CH_2Cl_2, scan rate 100 mV s^{-1}, Pt electrodes, ref. SCE).

Donor	λ_{max} (s) [nm]	ΔE [eV]	ε_{max} [$M^{-1}cm^{-1}$]	λ_{max}(f) [nm]	E_g [eV]	E_{pa} [V]	E_{pc} [V]	E_{HOMO} [eV] [a]	E_{LUMO} [eV] [b]
1	507	2.44	39000	520	2.00	1.32	-0.91	-6.01	-3.57
2	533	2.32	32000	542	1.86	1.02	-1.02	-5.71	-3.39
3	518	2.39	29000	532	1.92	1.15	-1.02	-5.84	-3.45
4	525	2.35	36000	520	2.01	1.11	-1.11	-5.80	-3.45
5	574	2.15	47000	560	1.75	0.79	-1.17	-5.48	-3.33
6	565	2.19	61000	585	1.84	0.90	-1.14	-5.76	-3.57
7	552	2.25	63000	562	1.88	0.93	-1.15	-5.79	-3.54

[a] using E^0_{ox} with an offset of -4.99 eV for SCE *vs* the vacuum level.[32]
[b] determined by E_{HOMO}-ΔE .

As shown by the data in table 1, the increase of the conjugation length and/or donor strength of the conjugating spacer produces a bathochromic shift of the absorption maximum (λ_{max}) of the ICT band from 507 to 574 nm for **1** and **5**, respectively with an increase of the molecular absorption coefficient (ε). The UV-Vis absorption spectra of thin-films cast on glass from chloroform solutions show in the case of derivatives **1-3**, **6** and **7** a bathochromic shift of λ_{max} and a broadening of the absorption band due to intermolecular interactions in the solid state. In contrast the solid-state spectra of the EDOT-containing compounds **4** and **5** show narrower absorption bands with a hypsochromic shift of λ_{max} in particular for compound **5** (14 nm) (table 1).

The intercept of the tangent to the long wavelength absorption edge of the film to the horizontal axis leads to estimated band gap values in the range 1.75–2.00 eV.

Electrochemical properties

The electrochemical properties of the compounds were analyzed by cyclic voltammetry (CV) in methylene chloride, in presence of 0.1M tetrabutylammonium hexafluorophosphate as supporting electrolyte. As expected, according to the UV-Vis

[32] D. Baran, A. Balan, S. Celebi, B. Meana Esteban, H. Neugebauer, N. S. Sariciftci, L. Toppare, *Chem. Mater.* **2010**, *22*, 2978.

absorption data, the anodic peak potentials (E_{pa}) decrease from 1.32 V for compound **1** to 0.79 V for compound **5** (table 1), reflecting the increase donor character of π-conjugated spacers. In the negative potential region, the CV of all compounds present an irreversible reduction wave with a cathodic peak potential (E_{pc}) varying from -0.91 V for compound **1** to -1.17 V for compound **5** (Table 1).

Evaluation of the photovoltaic properties

The potentialities of these compounds as donor materials for heterojunction solar cells have been evaluated in bilayer PHJ cells of 0.28 cm^2 active area with vacuum-deposited C_{60} as electron acceptor.

An interesting specificity of the new donors lies in the fact that their solubility, melting and decomposition temperatures are compatible with both solution-process and vacuum deposition. Note that in spite of good solubility, attempts to fabricate PHJ cells from a solution of derivative **3** remained unsuccessful due to inhomogeneity of the spin-cast film. Having little amount of donor materials **6** and **7**, the films of these derivatives were obtained only by the spin-coating method.

Using the vacuum-deposition process, the potentialities of compounds **1**, **2**, **4**, **5** as donor materials for heterojunction solar cells have been evaluated in two series of bilayer solar cells. For the first series of devices, *ca.* 15 nm thin film of the corresponding donor were deposited by thermal evaporation under vacuum while for the second series of devices, *ca.* 20 nm thin film were deposited. In all cases, better results were obtained with thinner films (15 nm) and after application of a 10 min. thermal treatment.

Figure 3 shows the current density *vs* voltage curves for the cells based on compounds **2** and **5** and the corresponding photovoltaic parameters for all compounds **1** - **7** are listed in table 2.

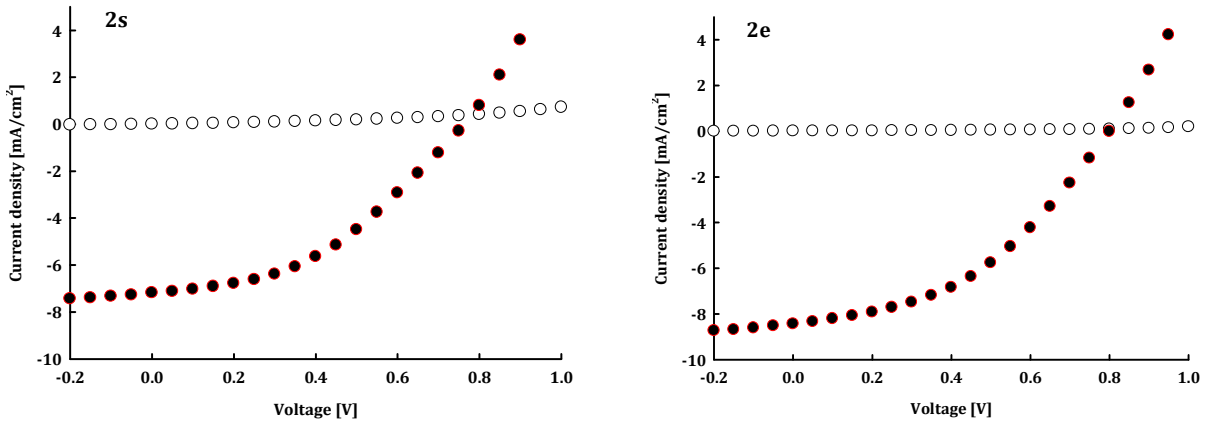

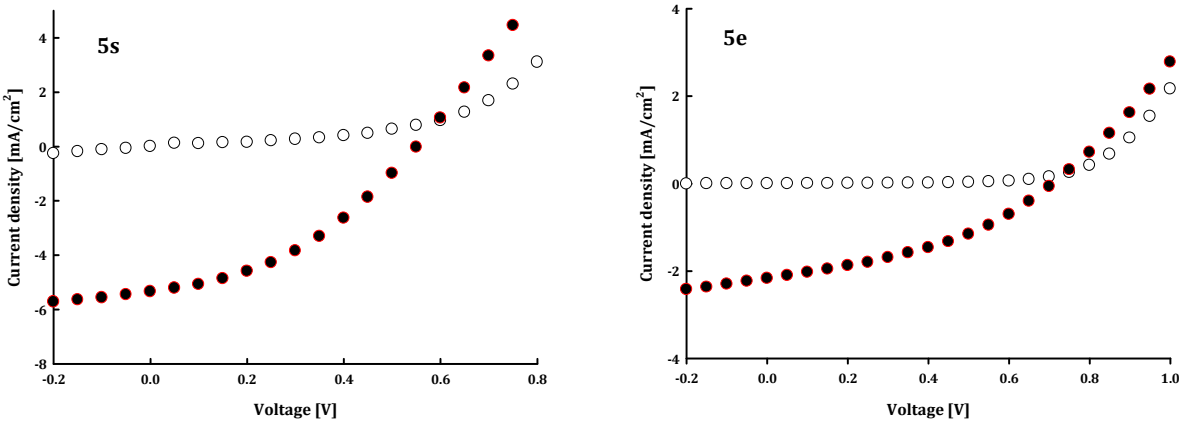

Figure 3. Current density *vs* voltage curves for a bilayer solar cell (ITO/PEDOT:PSS/**D**/C_{60}/aluminium). In the dark (open circles) and under simulated solar light with incident power light of 90 mW cm^{-2} (black circles).

Comparison of the results obtained with solution-cast and vacuum deposited donor layers reveals two contrasted behaviours. For compounds **1** and **2**, vacuum deposition improves J_{sc} while the reverse effect is observed for the EDOT-containing donors in particular for compound **5** for which vacuum-deposition leads to a considerable deterioration of the PV performances.

Table 2. Photovoltaic characteristics of PHJ bi-layer cells ITO/PEDOT:PSS/**D**/C_{60}/Al under AM 1.5 simulated solar light with an incident power light of 90 mW cm^{-2}. Data in italics are the average of 6-8 cells, data in bold are the best results for each series.

Compd	An. Temp [°C]	J_{sc} [mA cm^{-2}]	V_{oc} [V]	*FF* [%]	*PCE* [%]
1s	110	*6.40*	*0.75*	*33*	*1.76*
1s	110	**6.32**	**0.79**	**37**	**2.07**
1e	110	*6.83*	*0.68*	*32*	*1.64*
1e	110	**6.87**	**0.69**	**32**	**1.68**
2s	120	*7.32*	*0.74*	*40*	*2.41*
2s	120	**7.14**	**0.76**	**42**	**2.55**
2e	120	*8.73*	*0.77*	*40*	*3.06*
2e	120	**8.42**	**0.80**	**43**	**3.22**
3e	140	*7.71*	*0.61*	*41*	*2.15*
3e	140	**8.53**	**0.60**	**40**	**2.28**
4s	150	*5.68*	*0.66*	*29*	*1.28*
4s	150	**6.19**	**0.63**	**35**	**1.47**
4e	160	*4.78*	*0.69*	*29*	*1.05*
4e	160	**5.25**	**0.69**	**30**	**1.20**
5s	160	*5.65*	*0.63*	*32*	*1.22*

5s	160	**5.30**	**0.54**	**41**	**1.30**
5e	160	*2.12*	*0.66*	*39*	*0.63*
5e	160	**2.17**	**0.70**	**39**	**0.65**
6e	85	*2.92*	*0.67*	*22*	*0.47*
6e	85	**3.11**	**0.64**	**20**	**0.56**
7e	130	*5.47*	*0.52*	*29*	*0.92*
7e	130	**5.88**	**0.53**	**28**	**1.00**

In order to complete these observations, the external quantum efficiency (*EQE*) spectra of the cells have been recorded under monochromatic irradiation. The spectra of all devices show a first sharp peak at 370-380 nm assigned to the contribution of C_{60} to the photocurrent. The spectrum of the cells based on donor **2** shows as expected, an extension of the photo-response with a bathochromic shift of the onset of photo-current to ~650 nm. The *EQE* spectra of the cells based on solution-cast and vacuum-deposited donor layers are rather similar except for a slight higher intensity for the vacuum-deposited donor (figure 4).

As shown in figure 4, the processing technique has a much stronger effect in the case of EDOT-containing donors. For compound **5**, the spectra of the solution-processed and vacuum-deposited donors present as expected, an extension of the photo-response towards longer wavelengths. However, a marked decrease of *EQE* is observed in the 500-700 nm region for the vacuum-deposited donor. These *EQE* spectra agree well with the results obtained under white light illumination and clearly confirm the negative influence of the bis-EDOT spacer on the conversion efficiency of the donor molecule.

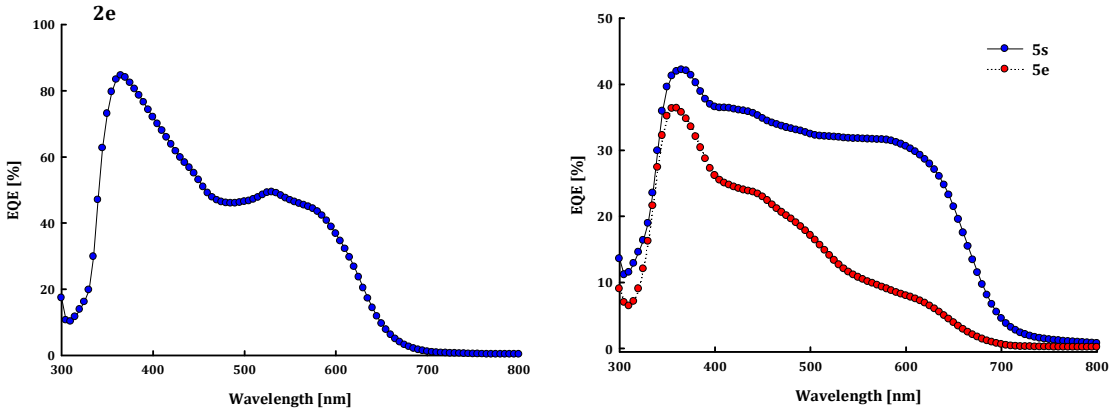

Figure 4. Spectra of external quantum efficiency of bi-layer cells based on donors **2** and **5** under monochromatic irradiation. (**s**) Spun-cast donor layer (**e**) vacuum-deposited donor layer.

Although our results confirm that depending on the molecular structure, the processing technique can exert a significant influence on the efficiency of the resulting OPV cell. Thus, whereas for compound **1** both methods lead to rather similar results, for

compound **2** vacuum deposition leads to a *ca* 25% increase of *PCE* due essentially to an increase of J_{sc}. In contrast, for compounds **4** and **5** vacuum-deposition seems to exalt the deleterious influence of the EDOT unit on molecular packing and hence PV performances.

4.2.2. Synthesis and characterization of new ADA, ADDA and ADADA systems based on triphenylamine

In our continuing interest for the manipulation of the electronic properties of type **8** compounds, we synthesised a series of donor-acceptor systems obtained by introduction of a spacer unit, such as ethynyl between the donor and acceptor (compound **9**), by extension of the basic structure either by simple dimerization leading to the A-D-D-A compound **10**, or by creation of a median acceptor linking group such as carbonyl, dicyanomethylene or cyanovinyl to form A-D-A-D-A structures **11-13** and A-D-A structure **14** (figure 5).

The reference compound **8** was obtained according to a known procedure described in the literature.[33] Compound **9** was obtained in a multi-step reaction procedure starting from commercially available 4-bromo-diphenylaniline **15** (scheme 2). Firstly, a Sonogashira cross-coupling reaction followed by trimethylsilyl deprotection reaction gave derivative **17** which was further subjected to another metal-catalysed Sonogashira reaction with 5-bromothiophene-2-carbaldehyde **18** yielding derivative **19** in good yield. Finally, a Knoevenagel condensation of aldehyde **19** with malonidinitrile gave the target compound **9** in 80% yield (scheme 2).

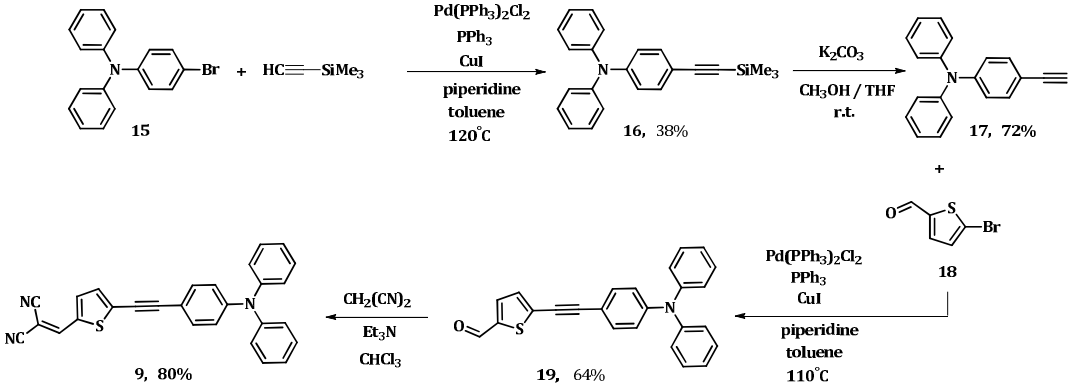

Scheme 2. Synthesis of derivative **9**

[33] A. Leliège, C.-H. Le Régent, M. Allain, P. Blanchard, J. Roncali, *Chem. Commun.* **2012**, *48*, 8907.

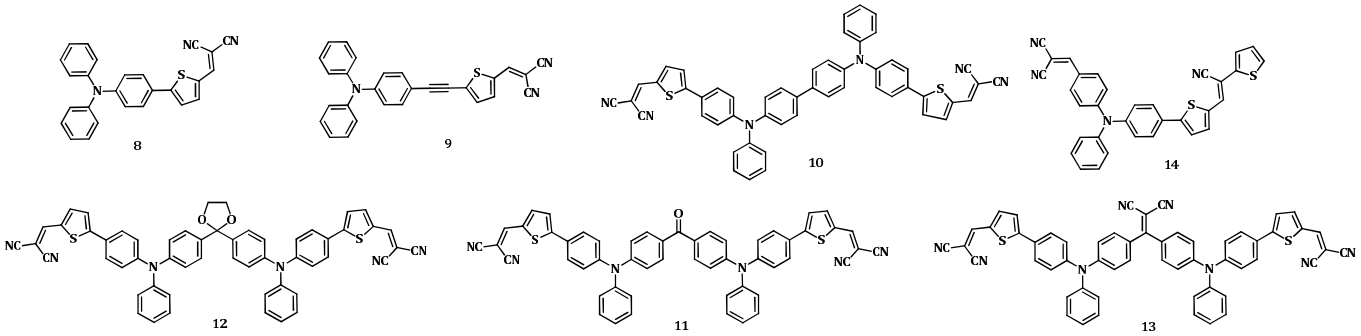

Figure 5. Chemical structures of target compounds

Compound **10** was prepared by oxidative coupling of **8** with copper perchlorate in acetonitrile at room temperature.[34] A Friedel-Craft reaction between compound **8** and oxalyl chloride gave ketone **11** in 68% yield (Scheme 3). A three-day reflux of **11** with ethylene glycol in the presence of *p*-toluene sulfonic acid using a Dean-Stark trap gave compound **12** in 46% yield. A Knoevenagel reaction of ketone **11** with malononitrile in the presence of $TiCl_4$ gave the dicyanovinyl derivative **13** in 45% yield.[35]

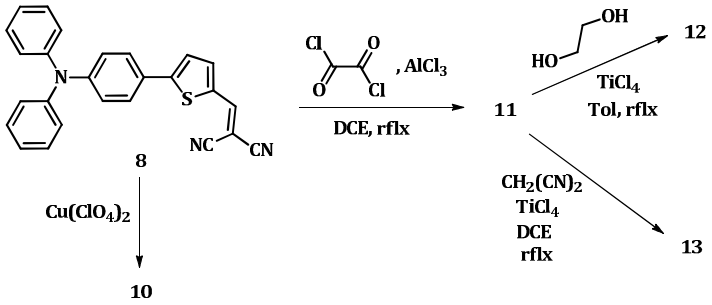

Scheme 3

Introduction of a cyanovinyl group between the donor and acceptor units helps to increase the intramolecular charge transfer and reduces also the optical band gap of the molecule.[36] In this context, attempts to synthesise a D-A-A system, such as compound **23** (scheme 4) failed because in the second step, the Vilsmeier-Haack formylation took place at *para*-position of phenyl ring instead of the free α-position of thiophene unit. Therefore, we obtained an A-D-A system instead of a D-A-A system. The X-ray analysis of compound **14** confirms the proposed structure (figure 6).

[34] K. Sreenath, C. V. Suneesh, V. K. R. Kumar, K. R. Gopidas, *J. Org. Chem.* **2008**, *73*, 3245.
[35] A. Diac, D. Demeter, S. Jungsuttiwong, I. Grosu, J. Roncali, *Tetrahedron Lett.* **2015**, *56*, 4607.
[36] (a) Y.-A. Duan, Y. Geng, H.-B. Li, X.-D. Tang, J.-L. Jin, Z.-M. Su, *Org. Electronics* **2012**, *13*, 1213; (b) S. Zeng, L. Yin, C. Ji, X. Jiang, K. Li, Y. Li, Y. Wang, *Chem. Commun*. **2012**, **48**, 10627.

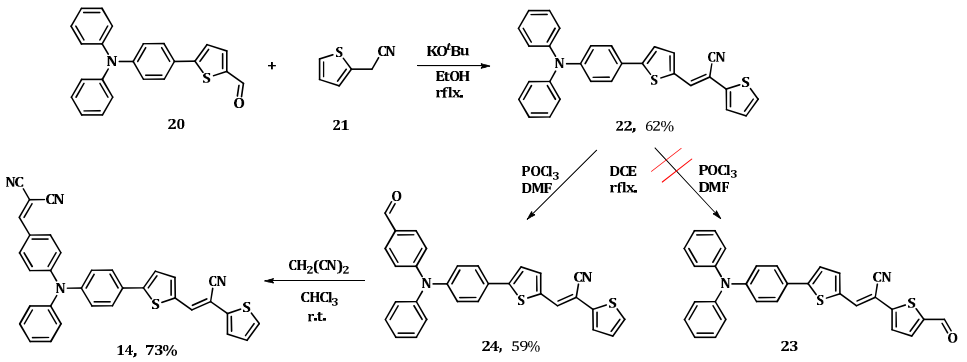

Scheme 4

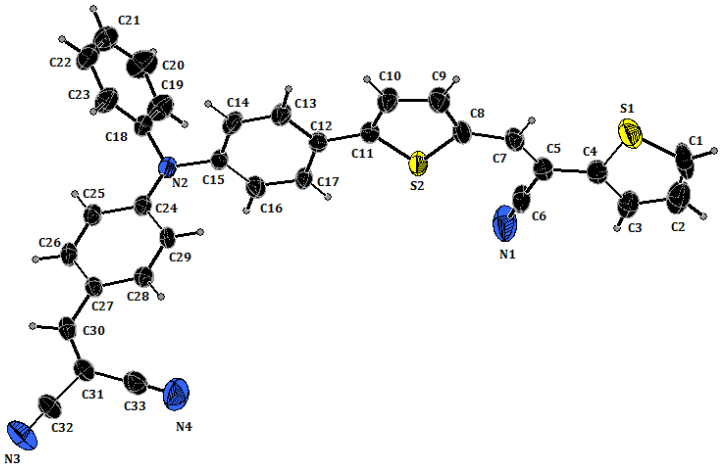

Figure 6. X-Ray single crystal structure **14**

Optical properties

The spectroscopic analysis of the molecules were performed in methylene chloride

Table 3. UV-Vis absorption spectroscopy data: (*s*: in CH_2Cl_2; *f*: thin films spun-cast on glass) and cyclic voltammetry (0.10 M Bu_4NPF_6/CH_2Cl_2, scan rate 100 mVs^{-1}, Pt electrodes, ref SCE) for compounds **8-14.**

Donor	λ_{max}^s [nm]	ε_{max} [$M^{-1}cm^{-1}$]	λ_{max}^f [nm]	E_g (eV)	$E_{pa}1, E_{pa}2$ [V]	E_{pc} [V]	E_{HOMO} (eV)[a]	E_{LUMO} (eV)[b]	E_{HOMO} (eV)[c]	E_{LUMO} (eV)[c]
8	502	36300	520	2.00	1.04	-1.10	-5.83	-3.36	-5.23	-2.80
9	493	44500	508	2.05	1.06	-1.03	-5.90	-3.38	-	-
10	510	63000	529	1.97	0.86, 1.05	-1.10	-5.74	-3.31	-5.10	-2.83
11	487	54000	492	2.10	1.19	-1.16	-5.96	-3.42	-5.35	-2.88
12	501	54000	515	2.12	1.04, 1.18	-1.12	-5.89	-3.42	-5.20	-2.82
13	489	78000	524	1.92	1.21	-1.31	-6.01	-3.48	-5.45	-2.94
14	496	50400	512	2.07	1.09, 1.38	-1.26	-5.92	-3.42	-	-

[a]Using E^0_{ox} with an offset of -4.99 eV for SCE vs the vacuum level. [b]Determined by E_{HOMO}-ΔE. [c] Calculated values

solutions and thin film spun-cast on glass from chloroform solutions. The spectrum of all compounds shows a first transition in the 350-400 nm region followed by a main absorption band with a maximum (λ_{max}) at ~500 nm assigned to an internal charge transfer (ICT). Comparison with compound **8** shows that except for compound **10** for which a small red shift of λ_{max} is observed, all the other compounds presents a small hypsochromic shift of λ_{max} along with an increase of the molecular absorption coefficient (ε) (table 3). UV-Vis spectra of the films present a red shift of λ_{max} and a broadening of the absorption band reflecting intermolecular interactions.

Electrochemical properties

The electrochemical properties of the final compounds have been analyzed by cyclic voltammetry in methylene chloride solutions in the presence of tetra-*n*-butyl ammonium hexafluorophosphate (*n*-Bu_4NPF_6) as supporting electrolyte. The CV of derivative **9** (figure 7) shows a reversible oxidation process corresponding to the formation of stable cation-radical with anodic peak potential E_{pa} at 1.06 V which is positively shifted (*ca.* 20 mV) compared to reference compound **8**.

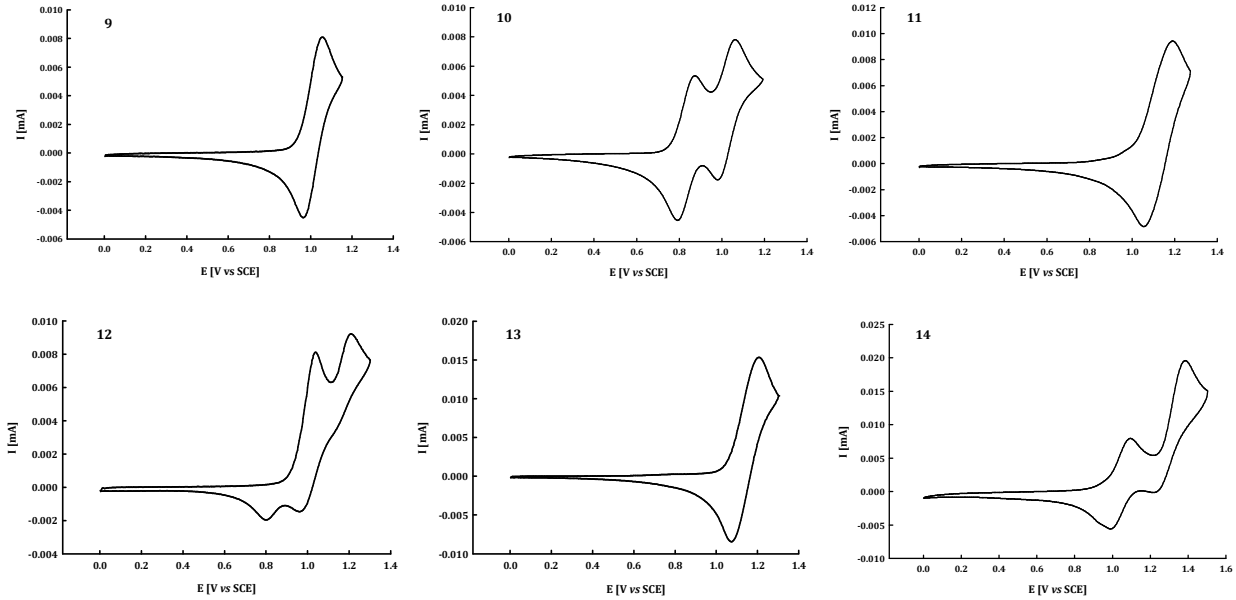

Figure 7. Cyclic voltammograms of compounds **9-14** in 0.10 M Bu_4NPF_6/CH_2Cl_2, Pt electrodes, scan rate = 100 mV s^{-1}.

The cyclic voltammogram (CV) of compound **10** shows two reversible one-electron oxidation waves with anodic peak potential E_{pa}^1 and E_{pa}^2 at 0.86 and 1.05 V (figure 7). Comparison with compound **8** reveals a 190 mV negative shift of E_{pa}^1 which reflects the extension of the conjugated system, in agreement with UV-Vis data. The second oxidation

process can be assigned either to the formation of a dication on the extended system or to the formation of a cation-radical on each part of the molecule. The CV of compound **11** shows a positive shift of E_{pa} to 1.19 V due to the electron-withdrawing effect of the carbonyl group. A similar effect is observed for compound **13** with E_{pa} increasing to 1.21 V. The CV of compound **12** shows some similarities with that of compound **10**, in particular the occurrence of two reversible oxidation steps with E_{pa}^1 and E_{pa}^2 at 1.04 and 1.18 V. In the positive potentials region, the CV of compound **14** exhibits two reversible one-electron oxidation waves at E_{pa}^1 = 1.09V and E_{pa}^2 = 1.38V assigned to the formation of stable cation-radical and dication.

In the negative potential region (not shown), the CV of all compounds displays an irreversible reduction process with cathodic peak potential (E_{pc}) in the -1.03V to -1.31V region indicative of unstable anion radical.

Theoretical calculations

To better understand the electronic structures, the geometry of derivatives **10**-**13** was optimized using density functional calculation methods.

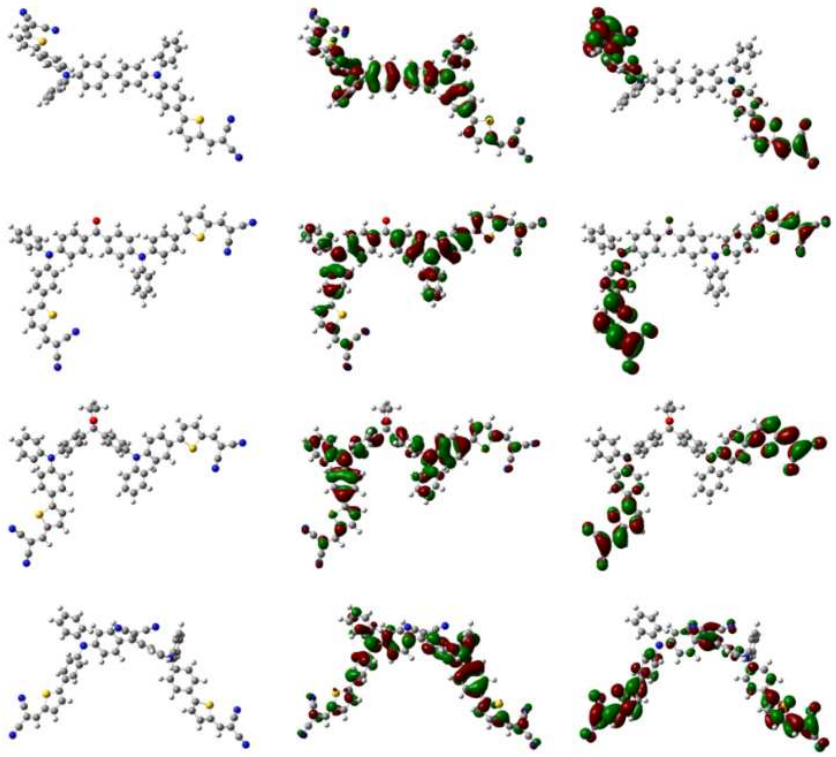

Figure 8. Molecular orbital surface of molecules **10-13** (from top to bottom) calculated by DFT/B3LYP/6-31G(d,p) with CH_2Cl_2 solvent (C-PCM model). Left: optimized geometry, middle HOMO, right: LUMO.

As expected, the HOMO is essentially distributed over the TPA blocks and the LUMO on the dicyanovinyl acceptor group. The introduction of a median electron-acceptor linking group does not significantly modify the distribution, except for compound **13** for which some LUMO coefficient also appear on the dicyanomethylene group.

The calculated values of the energy levels of the frontier orbitals and HOMO-LUMO gap agree well with experiments and confirm a slight increase of the HOMO for compounds **10** and **12** and a small decrease of HOMO and LUMO for **11** and **13** (table 3).

Evaluation of the photovoltaic properties

A preliminary evaluation of the new compounds as donor materials for OPV cells has been carried out on bi-layer planar heterojunction of 28 mm^2 active area.

The photovoltaic characteristics of the bi-layer cells based on the six donors are shown in figure 9 and the corresponding data are listed in table 5 using compound **8** as reference.

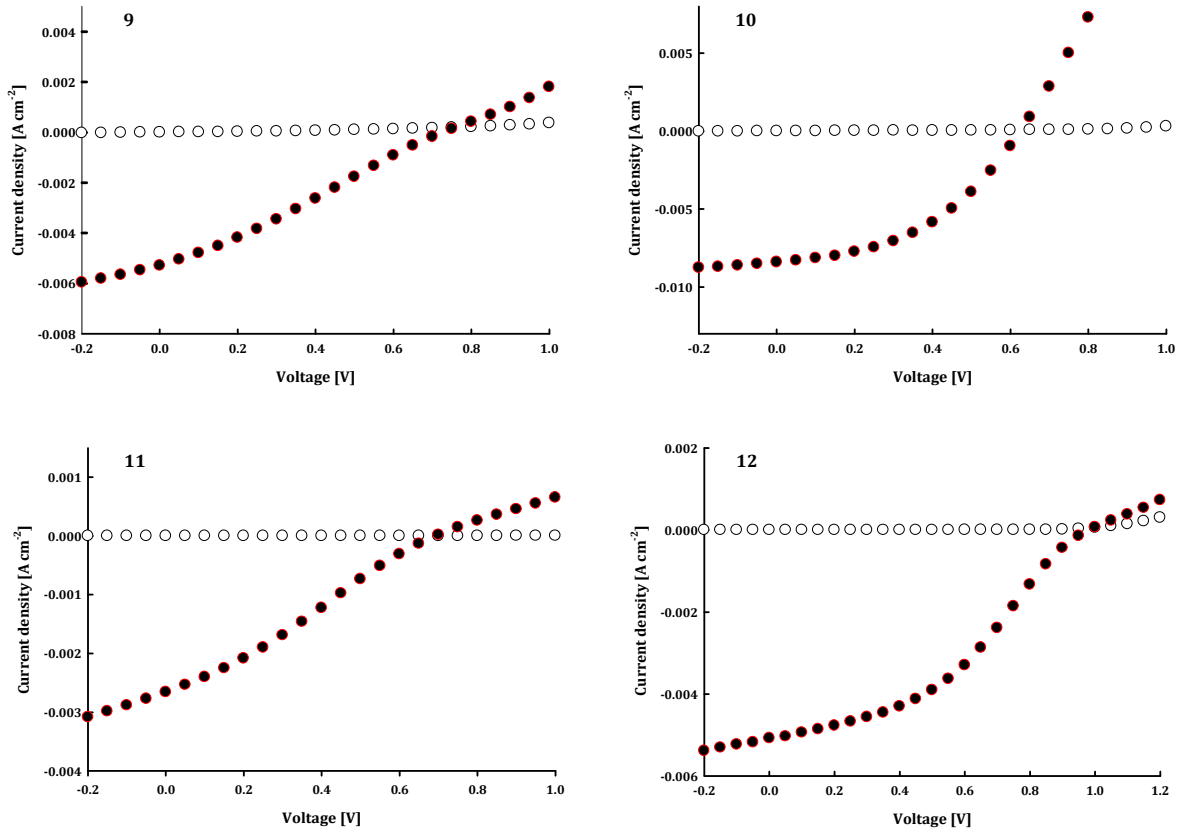

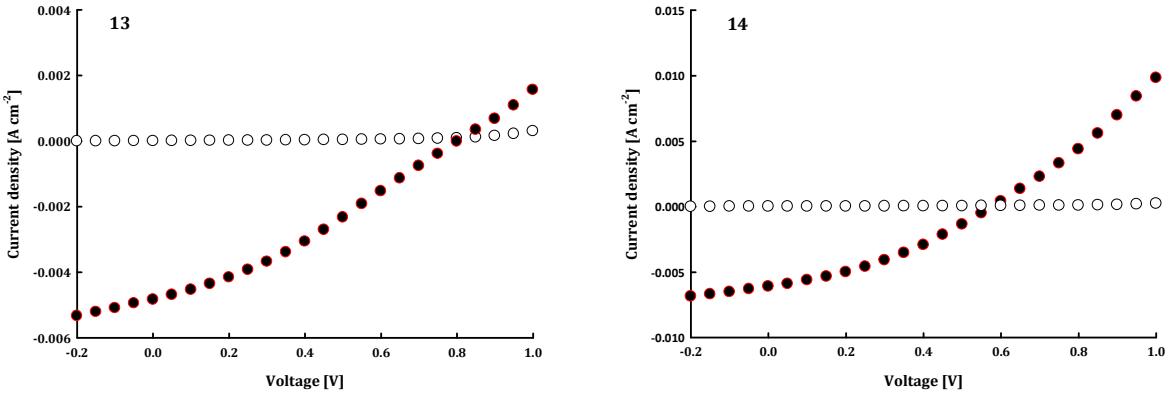

Figure 9. Current density *vs* voltage curves of bilayer cells ITO/PEDOT:PSS/donor/C_{60}/Al. In the dark (open circles) and under AM 1.5 simulated solar light (90 mW cm^{-2}) (black/red circles)

A first examination of the current density vs voltage curves of derivative **9** clearly shows that the introduction of an ethynyl group between the donor and acceptor units exerts a considerable effect on the performances of the cells. Thus, the *PCE* decreased from 2.50% for reference compound **8** to 1.28% for compound **9**.

Table 4. Photovoltaic characteristics of PHJ bi-layer cells ITO/PEDOT:PSS/**D**/C_{60}/Al under AM 1.5 simulated solar light with an incident power light of 90 mW cm^{-2}. Data in italics are the average of 6-8 cells, data in bold are the best results for each series.

Donor	J_{sc} [mA/cm²]	V_{oc} [V]	FF [%]	PCE [%]
8	5.77	0.92	52	2.50
9	*4.80*	*0.73*	*29*	*1.16*
9	**5.52**	**0.73**	**30**	**1.28**
10	*8.04*	*0.66*	*41*	*2.44*
10	**8.41**	**0.63**	**44**	**2.62**
11	*2.14*	*0.71*	*23*	*0.49*
11	**2.66**	**0.69**	**28**	**0.55**
12	*4.81*	*0.97*	*38*	*1.96*
12	**5.10**	**0.98**	**40**	**2.16**
13	*4.55*	*0.79*	*32*	*1.26*
13	**4.88**	**0.79**	**33**	**1.38**
14	*6.00*	*0.62*	*32*	*1.34*
14	**6.18**	**0.58**	**34**	**1.38**

The data in table 4 show that the introduction of a median carbonyl or dicyanomethylene acceptor group between the two blocks leads to a net decrease of *PCE* from 2.50% for **8** to 0.55 and 1.38% for **11** and **13**, respectively. This effect is due in particular to a decrease of the short-circuit current density (J_{sc}) and before all to low fill-factors *FF*. A lesser decrease of *PCE* is observed for **12** which is anyway less efficient that the reference compound **8**. On the other hand, a significant improvement of J_{sc} from 5.77 to 8.41 mA cm^{-2} is observed for donor **10** which results in slight increase of *PCE* in spite of a large decrease of open-circuit voltage (V_{oc}). This reduced voltage is related to the increase of the HOMO level caused by the extension of conjugation in **10**.

The results for compound **14** show that introduction of two acceptor groups on both sides of TPA block leads to a slight improvement of J_{sc} from 5.77 to 6.18 mA cm^{-2} but to a decrease of V_{oc} and FF with as net result a decrease of *PCE* to *ca.* 1.38%.

4.3. Conclusions

Donor-acceptor molecules (D-π-A) built by connecting a diphenylhydrazone block to a dicyanovinyl acceptor group *via* various thiophene-based π-conjugating spacers (**1-7**) have been synthesized from mono- or di-aldehydes by simple metal-free procedure. Cyclic voltammetry and UV-Vis absorption spectroscopy show that the conjugation extension and/or increase of the donor strength of the spacer produces a decrease of the HOMO and LUMO energy level, a red shift of the absorption spectrum and an increase of the molecular absorption coefficient. Compared to solutions, the optical spectra of spin-cast thin films of compounds **1-3**, **6**, **7** show a broadening and red shift of the absorption bands consistent with the formation of *J*-aggregates. In contrast, the blue shift observed for the EDOT-containing compounds **4** and **5** suggests the presence of *H*-aggregates.

A first evaluation of the potential applications of the compounds as donor materials in simple bi-layer cells has confirmed the determining role of the conjugating bridge on conversion efficiency. The results obtained with EDOT-containing molecules have confirmed the difficulty to predict the effects of this building block on the organization of the material and hence on its electronic properties and photovoltaic performances. On the other hand, the results obtained with donors based on thiophenic spacers and in particular a bithiophene suggest that these materials can represent an interesting trade-off when one considers the balance of the relevant OPV parameters namely, cost, simplicity, cleanness, yield and scalability of the synthesis and conversion efficiency. Furthermore, the possibility to process these materials by both solution process and vacuum deposition appears as an additional interesting characteristic.

Six molecular donor (D) acceptor (A) systems of structure D-π-A (**9**), A-D-A-D-A (**11**-**13**), A-D-D-A (**10**) and A-D-A (**14**) have been synthesized by spatial extension of a reference D-A system with a triphenylamine donor block (**8**). UV-Vis absorption spectroscopy, cyclic voltammetry and theoretical calculations show that the presence of a

median acceptor group has limited effect on the internal charge transfer while direct dimerization leads to an increase of the effective conjugation length. A cursory evaluation of the new compounds as donor material in bilayer solar cells using fullerene C_{60} as acceptor material shows that the presence of a median acceptor has deleterious effect on conversion efficiency while the simple dimerization of the molecule leads to a substantial improvement of short-circuit current density with a moderate improvement of conversion efficiency.

Chapter 5: Electroluminescent Carbon 'Quantum' Dots : a New Concept for Next Generation Optoelectronic Devices

5.1. Introduction

Carbon quantum dots have emerged as alternative fluorescent nanoprobes due to their availability, thermal stability and relatively non-cytotoxic nature.[37,38] Versatile applications of CDs include bioimaging,[39] catalysis,[40] and photoreduction of metals,[41] due to the high electron donor–acceptor ability.

5.2. Original Contributions

One objective of this research work is the synthesis and characterization of CDs passivated with small organic molecules such as 1,3-propanediamine (CDs-PD), *p*-phenylenediamine (CDs-PPD), and also polymers like PEG_{1500N} (CDs-PEG_{1500N}).

Another objective is the investigation of electroluminescence properties of CDs in LED devices and, on the other hand, the potential of CDs to function as energy donors by covalently attaching rhodamine B (RhB) to the free amino group of CDs-PEG_{1500N}.

It is well known that the fluorescence quantum yield of carbon nanoparticles is significantly enhanced by their functionalization with oligomers and polymers. In this context, the surface defects on the carbon nanoparticles were passivated with both small molecules and oligomers.

The commercially supplied carbon nanoparticles were refluxed in an aqueous nitric acid solution (2.6M) in order to oxidize some of the surface carbons into carboxylic acids. The resulting nanoparticles were subsequently dialyzed against deionized water and then gravimetrically fractionated for harvesting the smaller nanoparticles. The as-obtained samples still exhibited no detectable photoluminescence. However, upon surface

---

[37] S. T. Yang, X.Wang, H. Wang, F. Lu, P. G.Luo, L. Cao, M. J. Meziani, J. H. Liu, Y. Liu,M. Chen, Y. Huang, Y. P. Sun, *J. Phys. Chem. C* **2009**, *113*, 18110.

[38] S. C. Ray, A. Saha, N. R. Jana, R. Sarkar, *J. Phys. Chem. C* **2009**, *113*, 18546.

[39] C.Liu, P. Zhang, F. Tian, W.Li, F.Li, W.Liu, *J. Mater. Chem*. **2011**, *21*, 13163.

[40] S. Mitra, S. Chandra, P. Patra, P. Pramanik, A. Goswami, *J. Mater. Chem*. **2011**, *21*, 17638.

[41] X. Wang, L. Cao, F. S. Lu, M. J.Meziani, H. Li, G. Qi, B. Zhou, B. A. Harruff, F. Kermarrec, Y. P. Sun, *Chem. Commun*. **2009**, *25*, 3774.

passivation by attaching simple organic species to the acid-treated carbon particles (scheme 1), bright luminescence emissions were observed when irradiated at 365 nm (figure 1).

In this regard, upon being recovered from aqueous solution, the nanoparticles were further refluxed in neat thionyl chloride for the subsequent amidation reaction with small aliphatic diamine derivatives such as 1,3-propandiamine as well as aromatic diamine, *p*-phenylenediamine, and also with oligomeric poly(ethylene glycol)diamine (PEG_{1500N}). After the reaction time elapsed, the mixture was cooled to room temperature, dispersed in deionizated water and centrifuged to 25000*g* to retain the supernatant. The solution was further dialyzed against deionizated water to remove the free functional moieties and finally the as-prepared samples were fractionated on a gel column (Sephadex™ G-100) to harvest the most fluorescent fraction from each of the samples. The CDs-PD, CDs-PPD and CDs-PEG_{1500N} were obtained as colored aqueous solutions.

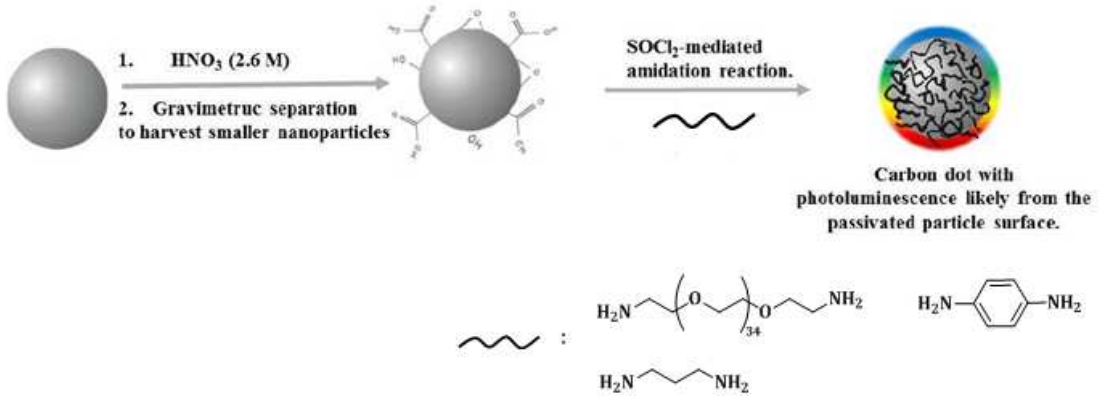

Scheme 1. Schematic representation of the process steps used to synthesize amine-functionalized CDs

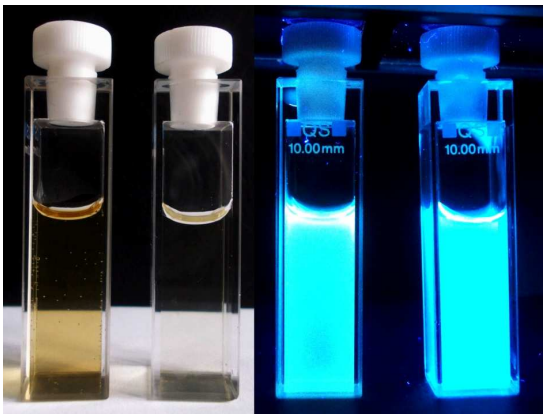

Figure 1. Aqueous solution of CDs-PEG_{1500N} and CDs-PD under normal light conditions (left) and under irradiation at 365 nm (right)

The optical absorption spectra of all obtained CDs are shown in figure 2, depicting the typical π-plasmon transitions in the core carbon nanoparticle. The fluorescence spectra also displayed characteristic CDs behavior, in that the emission maxima were progressively red-shifted with the spectral band becoming narrower and reduced in intensity with increasing excitation wavelength (figure 2). Nevertheless, the observed emission spectra corresponding to multiple excitation wavelengths covere the entire visible spectral region (figure 2). The photoluminescence quantum yields of the CDs-PD, CDs-PPD and CDs-PEG_{1500N} in aqueous solutions were about 9%, 14% and 10%, respectively (375–425 nm excitation, using the quinine sulphate standard).

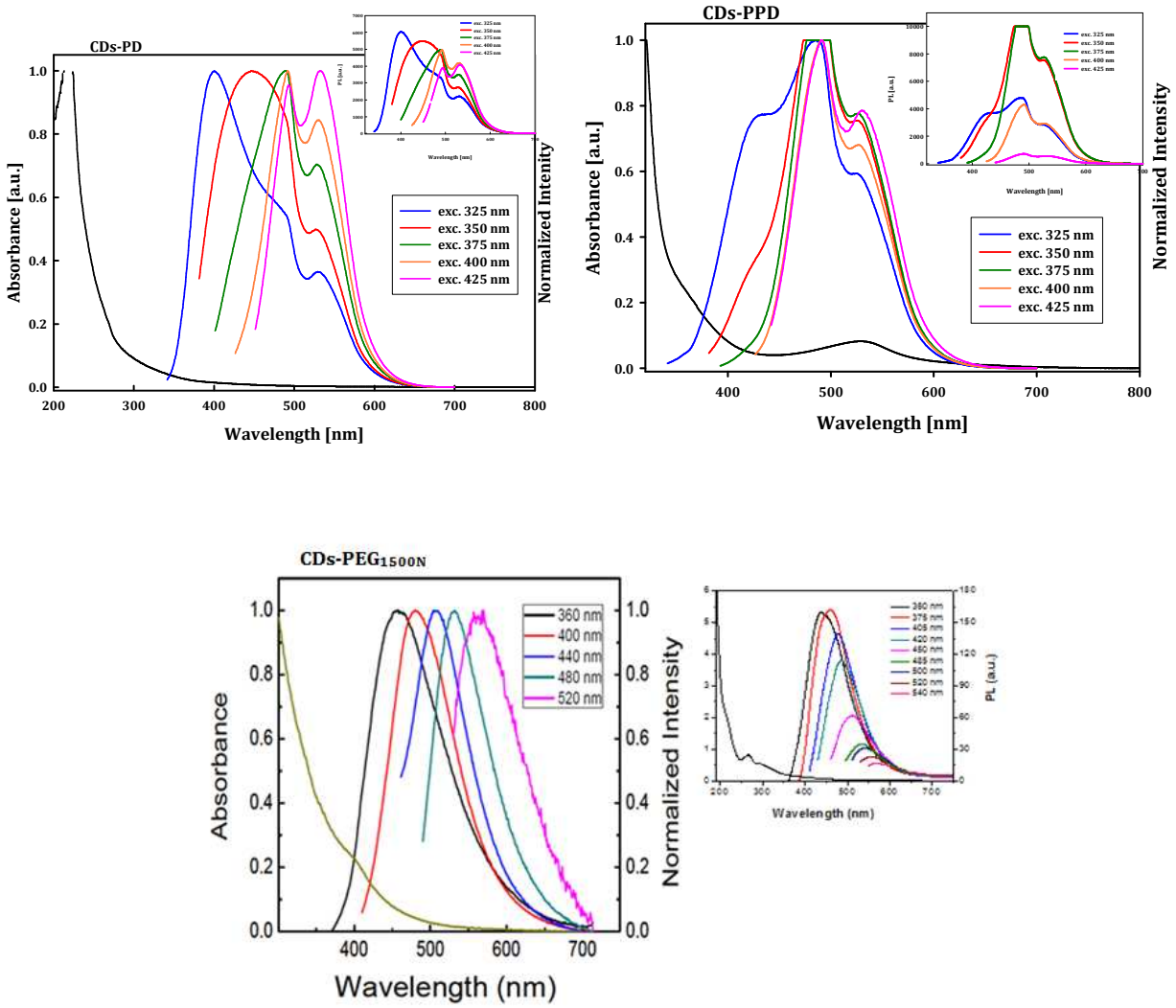

Figure 2. Absorption and normalized photoluminescence spectra (at different excitation wavelengths as listed) of CDs-PD (left), CDs-PPD (right) and CDs-PEG_{1500N} (bottom) in aqueous solution

The morphology of the passivated CDs-PEG$_{1500N}$ was established using high-resolution transmission electron microscopy (HR–TEM) which has revealed a crystalline structure with an average diameter of about 3.5 nm (figure 3).

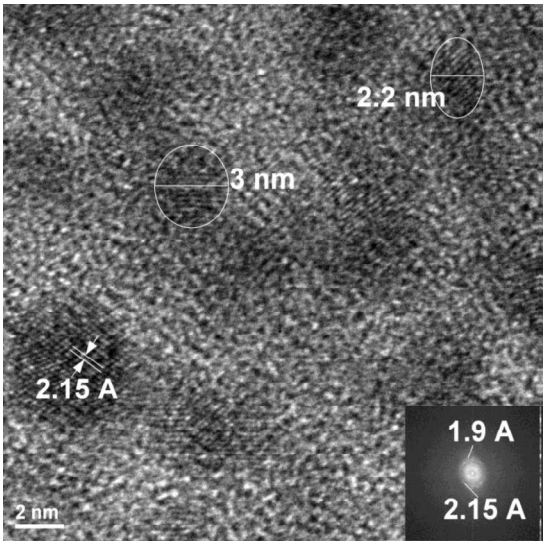

Figure 3. HR–TEM image of CDs-PEG$_{1500N}$

In the next step, we investigated the potential of CDs to act as energy donors in FRET by covalently attaching rhodamine B to the free amino group of the passivating polymer in CDs-PEG$_{1500N}$.

In this context, we subsequently used CDs-PEG$_{1500N}$ as donor in presence of RhB as acceptor, taking into account their good emission spectral overlap with the absorption of RhB, a condition required for high energy transfer efficiency. Figure 4 shows the spectral relationship between the UV-Vis absorption band of RhB and photoluminescence band of CDs-PEG$_{1500N}$ at different excitation wavelengths (as listed).

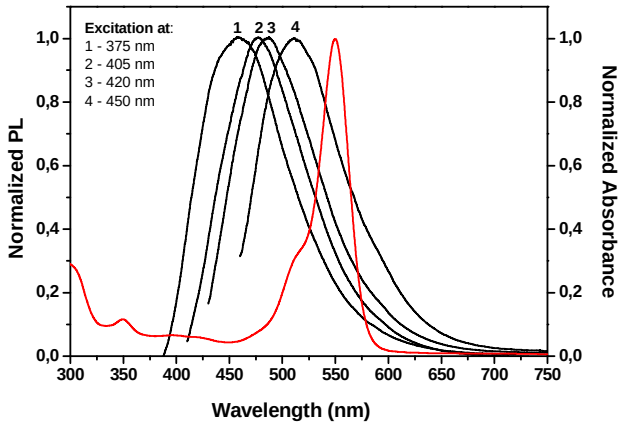

Figure 4. Spectral overlap of the normalized RhB absorption and CDs-PEG$_{1500N}$ photoluminescence

The covalent linkage of rhodamine B onto the surface of the CDs-PEG_{1500N} has been carried out after several successive reactions, which are depicted in scheme 2. The first three steps regarding the passivation of surface defects on carbon nanoparticles were already described in the first part of this chapter. The final step corresponds to the reaction with RhB isothiocyanate under alkaline anhydrous conditions to the primary amine groups of CDs-PEG_{1500N}.

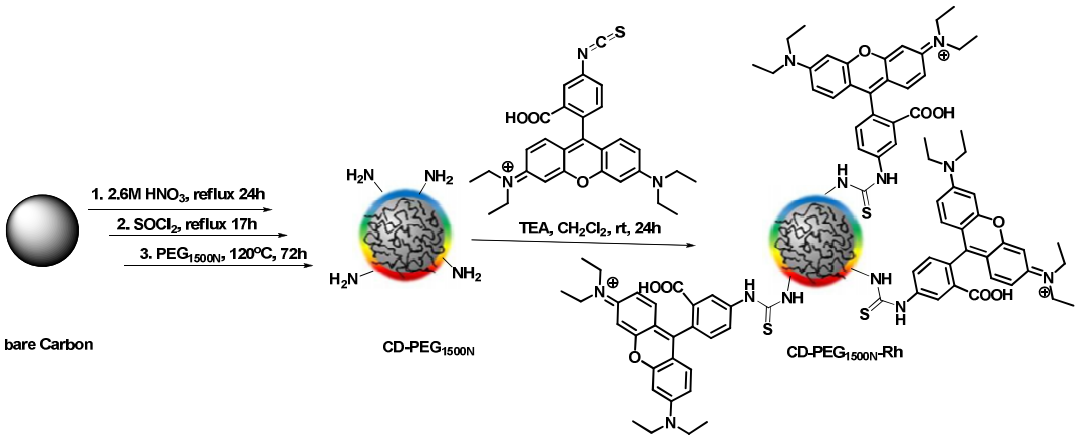

Scheme 2. Schematic illustration of the surface coupling process of CDs-PEG_{1500N} with RhB

The successful covalent attachment of the RhB was confirmed using FT-IR spectroscopy that indicated that the isothiocyanate moiety was converted into thiourea upon reaction with the terminal primary amine in the CDs-PEG_{1500N} (figure 5). The FT-IR spectrum of the CD-PEG_{1500N}-RhB shows the disaapearing of the absorption band at 2150 cm^{-1} corresponding to the asymmetric stretching mode in –N=C=S[42], indicating thus the covalent linkage of RhB to the terminal amine moiety of the CDs-PEG_{1500N}.

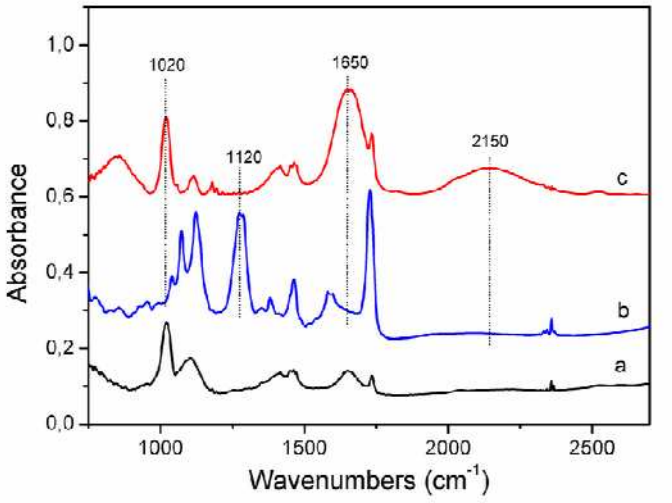

Figure 5. FT-IR spectra of (a) CDs-PEG_{1500N}; (b) CD-PEG_{1500N}-Rh and (c) RhB

[42] M. K. Murali, V. Balachandranb, *Indian J. Pure Appl. Phys.* **2012**, *50*, 19.

By comparing the UV-Vis absorption spectra of RhB and CD-PEG$_{1500N}$-Rh conjugate, a slight blue shift (2 nm) can be observed in the latter case, most probably due to the modifications of molecular structure (figure 6).

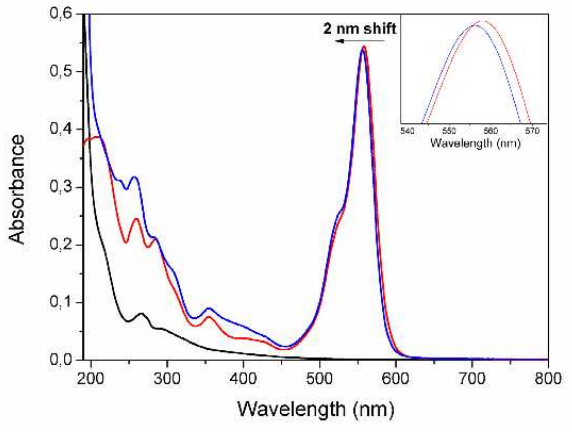

Figure 6. UV-Vis absorption spectra of CDs-PEG$_{1500N}$ (black spectrum), RhB (red spectrum) and CD-PEG$_{1500N}$-Rh (blue spectrum) recorded in water

We investigated further the photoluminescence properties of covalently bound RhB molecule to CDs-PEG$_{1500N}$ by steady-state and time-resolved photoluminescence measurements. Figure 7 displays the recorded photoluminescence spectra of CD-PEG$_{1500N}$-Rh conjugates excited at 375 nm, 405 nm, 420 nm and 450 nm together with the corresponding photoluminescence spectra of RhB and unconjugated CDs-PEG$_{1500N}$, of identical concentrations with those found in the conjugated system.

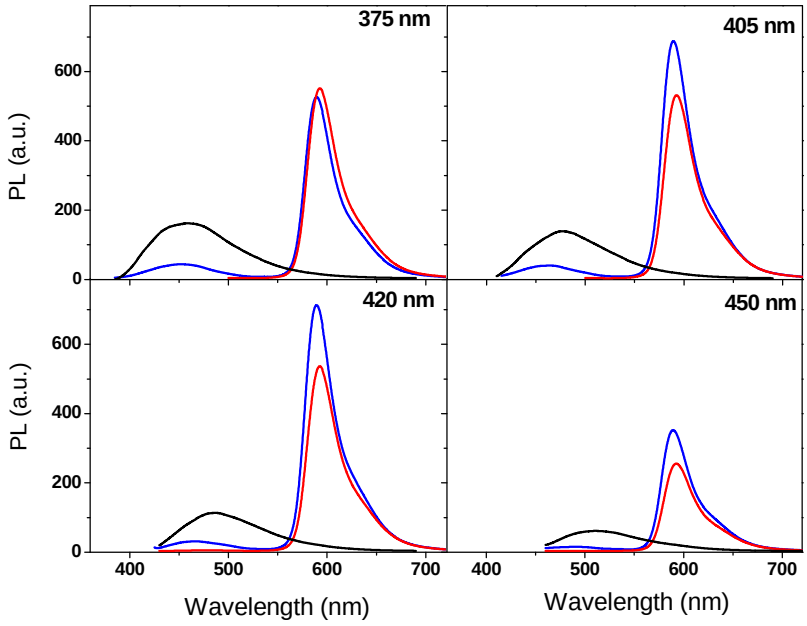

Figure 7. Comparison between the photoluminescence spectra of CDs-PEG$_{1500N}$ (black curves), CD-PEG$_{1500N}$-Rh (blue curves) and RhB (red curves) at indicated excitation wavelengths

As expected, the CD-PEG_{1500N}-Rh conjugates present two photoluminescence bands: at 450 nm assigned to CDs-PEG_{1500N} and 593 nm characteristic to RhB. Similar to UV-Vis absorption spectra discussed above, we noticed a blue-shift of RhB emission from 593 nm to 589 nm as an indication of conjugates formation.

Note that the intensity of CDs-PEG_{1500N} photoluminescence band decreases along with the increase of photoluminescence band of RhB dye at the selected excitation wavelengths (figure 7). This behavior is a clear signature of FRET mechanism, which operates between CDs-PEG_{1500N} as donor and RhB as acceptor. The highest FRET efficiency concluded from the increase of photoluminescence band of RhB occurs at 450 nm excitation wavelength, where the overlap between the absorbtion band of RhB dye and the photoluminescence band of CDs-PEG_{1500N} is maximum (figure 4).

An alternative method to quantify the efficiency of energy transfer between CDs and Rh molecules in CD-PEG_{1500N}-Rh conjugates is the determination of fluorescence lifetime of both emissive species.

Tail fitting operations revealed that the decay curve of CDs-PEG_{1500N} exhibits a long lifetime component of 6.5 ns (66.5%) and a shorter one of 1.8 ns (33.5%, table 1).

Table 1. Fluorescence decay parameters of CDs-PEG_{1500N} and CD-PEG_{1500N}-Rh solutions.

Sample	τ_1 (ns)	A_1 (%)	τ_2 (ns)	A_2 (%)	τ_{avg} (ns)	χ^2
CDs – PEG_{1500N}	6.5	66.5	1.8	33.5	4.9	1.05
CD – PEG_{1500N} – Rh	5.4	60.3	1.3	39.7	3.8	0.99

τ_n and A_n are the lifetime and amplitude of the n^{th} component; τ_{avg} is the amplitude-weighted average lifetime calculated with: $\tau_{avg} = \frac{\sum \tau_i * A_i}{\sum A_i}$; χ^2 - indicates the goodness of fit (1 shows a perfect fit).

The performed measurements on the conjugates reveal that both the exciton emission and surface trapped states of CDs-PEG_{1500N} are affected by the presence of Rh B dye. Specifically, we observed the decrease of lifetime components from 6.5 ns and 1.8 ns to 5.4 ns and 1.3 ns, respectively, as detailed in table 2. Consequently, the average lifetime of CDs-PEG_{1500N} decreased from 4.9 ns to 3.8 ns upon conjugation with Rh B acceptor molecules (see table 1). Shortening of the lifetime of CDs-PEG_{1500N} confirms an efficient energy transfer in our donor-acceptor system, in agreement with the previous results obtained from steady-state fluorescence measurements.

Furthermore, we have calculated the FRET efficiency and the rate of energy transfer in our system at 405 nm. Results are listed in table 2, along with the obtained Förster distance and the estimated distance between donor and acceptor.

Table 2. Parameters calculated for CD – PEG_{1500N} – Rh conjugates at 405 nm excitation.

Excitation wavelength (nm)	**Förster distance R_0** (Å)	τ_D (ns)	τ_{DA} (ns)	**FRET efficiency**	**D-A distance r** (Å)	**Energy transfer rate k_{DA}** (ns^{-1})	**Donor QY**
405	43.34	4.9	3.8	0.22	53.7	0.056	0.17

The unique excited state redox processes of CDs responsible for the luminescence emissions were further investigated by integration of CDs-PEG_{1500N} into multilayer light emitting diode devices.[43]

The LED device of a multilayer structure (ITO/PEDOT:PSS/PVK/carbon dots/Al, figure 8) was constructed by our partners at IMT Bucharest by sequentially spin-coating each layer from orthogonal solvents on top of the ITO substrate, with the Al cathode as the final layer deposited by thermal evaporation method through a shadow mask.

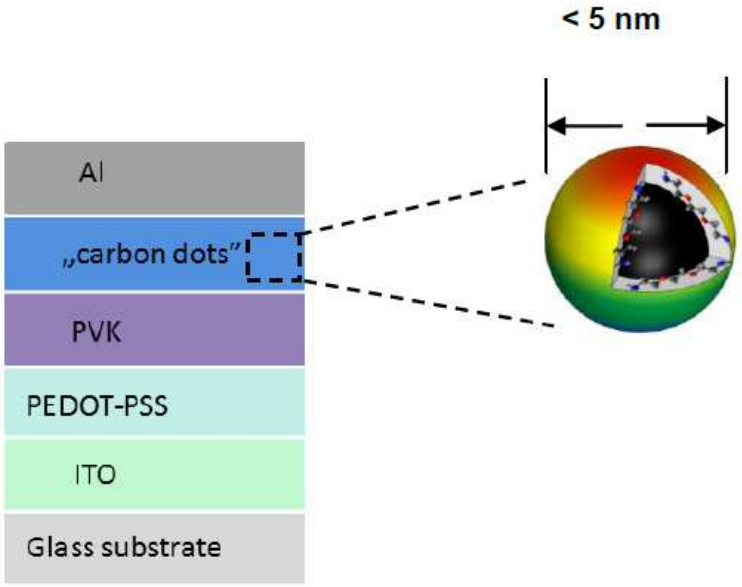

Figure 8. Carbon quantum dot diode – the architecture of the device with the ITO (anode), PEDOT:PSS (HIL), PVK (HTL), CDs (EL), Al (cathode)

The LED device was evaluated by applying a forward bias on the hole-injecting contact (HIL, ITO/PEDOT:PSS). With the external bias, electrons and holes were injected to result in the formation of excitons, from which the positive and negative polarons could radiatively recombine in the carbon dots layer for luminescence emissions.

The electroluminescence from the device was naked eye visible, as white light with a bluish color (figure 9). As it can be observed in figure 9a, the electroluminescence spectrum is broad and covers a wide range of the visible spectral region. On the other hand, the

[43] L. M. Veca, A. Diac, I. Mihalache, P. Wang, G. E. LeCroy, E. M. Pavelescu, R. Gavrila, E. Vasile, A. Terec, Y.-P. Sun, *Chem. Phys. Lett.* **2014**, *613*, 40.

electroluminescence spectra were not sensitive to variations of the applied voltage, 11–15V region (figure 9a). The chromaticity CIE coordinate (0.25, 0.24) for 15V applied biases was calculated from the electroluminescence spectrum (figure 9b).

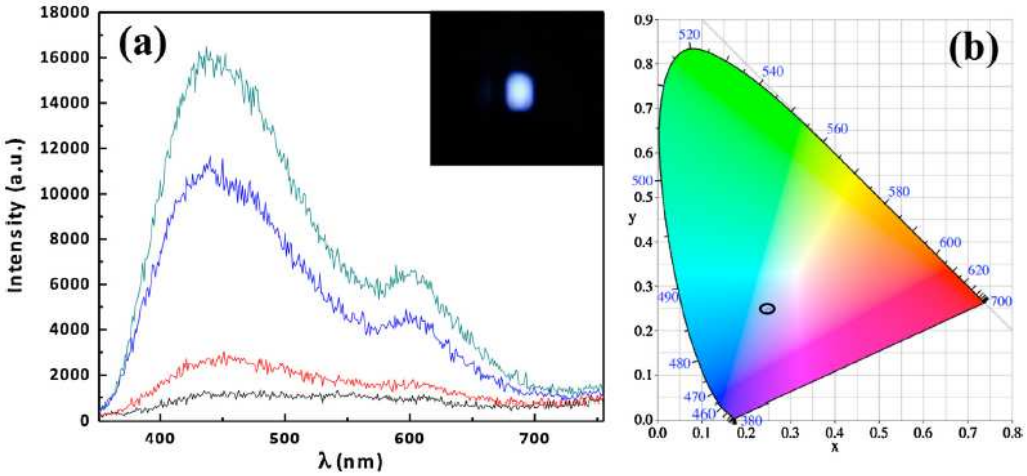

Figure 9. (a) Electroluminescence spectra of the device described in Fig. 11 at 10 V, 11 V, 13 V, and 15 V applied bias and (b) the CIE coordinates of the LED with carbon quantum dots as active layer, operated at 15 V and 5 mA. The inset shows a picture of the device at 20 V applied bias.

The general overlap between the electroluminescence spectrum and the collection of multiple photoluminescence spectra (obtained with multiple excitation wavelengths) seems to suggest that the recombination zone is within the carbon dots layer, with the PVK layer serving primarily the function of hole-transport (figure 10).

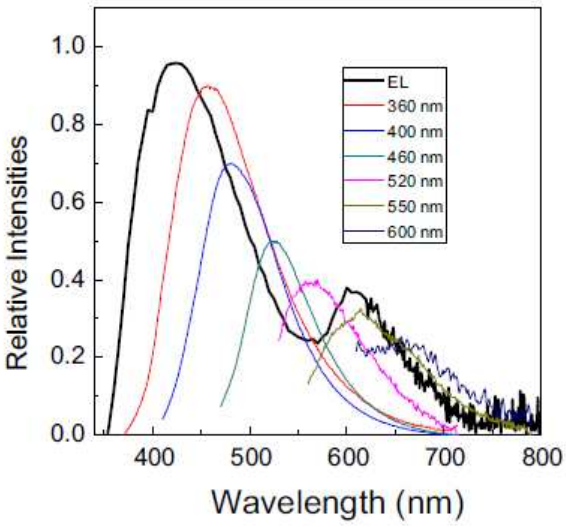

Figure 10. A comparison between the electroluminescence (EL) spectrum from theLED device with the PEGylated carbon dots and the corresponding photoluminescence spectra at the listed excitation wavelengths.

In quantum efficiency measurements, the emission signal was maximized by minimizing the distance between the emitting surface and a large area detector (detector

active area 100 mm^2 Ophirsilicon photodiode type PD300–3W). The LED device was operated at 15 V (current up to 5 mA), and the recorded power at 440 nm was 130 nW. Thus, the 'wall-plug efficiency' of the LED device was estimated (as the ratio of the measured power to the input power) to be 1.73×10^{-6}.

5.3. Conclusions

Three fluorescent carbon quantum dots materials were obtained by simple passivation of carbon nanoparticles surface with aromatic and aliphatic diamine derivatives, such as *p*-phenylenediamine, 1,3-propanediamine and oligomeric poly(ethylene glycol)diamine (PEG_{1500N}).

Carbon dots functionalized with Rhodamine B (CD-PEG_{1500N}-Rh), were synthesized by covalently attaching Rhodamine B to the free amino group of the passivating polymer in CDs-PEG_{1500N}. The covalent linkage of Rhodamine B to the carbon dots surface led to a non-radiative transfer of energy (FRET) from the CDs to the dye molecule. The efficiency of FRET was quantified by performing steady-state, along with life-time fluorescence measurements of both emissive species. The synthetic accessibility and the transfer efficiency of these conjugates make them reliable candidates for fluorescent materials, which could be later used in sensing and solar cells.

The electroluminescence properties of the carbon dots were investigated in multilayer light emitting diodes that use carbon dots as active layer. The devices emitted white light with a slight blue color, visible to the naked eye, suggesting that the carbon dots may potentially serve as a new platform for electroluminescent nanomaterials.

Future work will focus on the development of carbon dots with a shorter-chain surface passivation molecule, which would lead to an increased LED efficiency at a lower operating voltage for the corresponding devices.

General Conclusions

The thesis entitled "Design, Synthesis and Supramolecular Architectures of New Heterocyclic Compounds with Potential Applications in Material Chemistry and Photovoltaic Conversion" is structured into five chapters concerning new: a) heterocyclic cyclopenta[*c*]pyrans; b) indenopyrone derivatives with fluorescent properties; c) architectures based on cyclopenta[*c*]pyran unit as potential devices of molecular electronics; d) systems based on *N,N'*-diphenylhydrazone and triphenylamine as molecular donors for organic photovoltaics and e) electroluminescent carbon 'quantum' dots.

The different topics developed in this work have in common the willingness to develop new π-conjugated systems potentially useful as active materials for molecular electronics, organic solar cells and light emitting diodes.

The first chapter presents a study of pseudoazulene derivatives having a cyclopenta[*c*]pyran unit. The survey comprises the synthesis, structural analysis and reactivity towards electrophilic substitution in order to obtain fluorescent compounds. By following a multi-step strategy which starts from 1,3,4-oxadiazin-6-ones, six new series of cyclopenta[*c*]pyran derivatives were obtained and investigated using 1D, 2D NMR, UV-Vis/fluorescence spectroscopy, mass spectrometry, cyclic voltammetry and X-Ray diffractometry.

The second chapter deals with the investigation of some new indenopyrone derivatives, including separation of regio- and diastereoisomers, study of their fluorescent properties and determination of fluorescence quantum yield.

Two series of molecular systems based on terpyridine and phenothiazine blocks have been synthesized and completely analyzed by NMR, UV-Vis, fluorescence spectroscopy and mass spectrometry. Attempts have been made to determine the application of these systems in molecular electronics as potential logic gates. We obtained a system able to mimic an 'OR' gate.

Donor-acceptor molecules (D-π-A) built by connecting a diphenylhydrazone block to a dicyanovinyl acceptor group *via* various thiophene-based π-conjugating spacers have been synthesized from mono- or di-aldehydes by simple metal-free procedure. Cyclic voltammetry and UV-Vis absorption spectroscopy show that the extension and/or increase of the donor strength of the spacer produces a decrease of the HOMO and LUMO energy level, a red shift of the absorption spectrum and an increase of the molecular absorption coefficient. A first evaluation of the potential of the compounds as donor material in simple bi-layer cells has confirmed the determining role of the conjugating bridge on conversion efficiency. Furthermore, new ADDA and ADADA systems based on triphenylamine as molecular donors for organic solar cells (OSCs) were obtained. UV-Vis absorption spectroscopy, cyclic voltammetry and theoretical calculations show that the presence of a median acceptor group has limited effect on the internal charge transfer while direct dimerization leads to an increase of the effective conjugation length. A cursory evaluation of the new compounds as donor material in bilayer solar cells using fullerene C_{60} as acceptor material shows that the presence of a median acceptor has deleterious effect on conversion efficiency while the simple dimerization of the molecule leads to a substantial improvement of short-circuit current density with a moderate improvement of conversion efficiency.

In the last chapter three fluorescent carbon quantum dots materials were obtained by simple passivation of carbon nanoparticles surface with aromatic and aliphatic diamine derivatives, such as *p*-phenylenediamine, 1,3-propanediamine and oligomeric poly(ethylene glycol)diamine (PEG_{1500N}). Carbon dots functionalized with Rhodamine B (CD-PEG_{1500N}-Rh) were synthesized by covalently attaching Rhodamine B to the free amino group of the passivating polymer in CDs-PEG_{1500N}. The covalent linkage of Rhodamine B to the carbon dots surface led to a non-radiative transfer of energy (FRET) from the CDs to the

dye molecule. The electroluminescence properties of the carbon dots were investigated in a multilayer light emitting diode that use carbon dots as active layer. The device emitted white light with a slight blue color, visible to naked eyes, suggesting that the carbon dots may potentially serve as a new platform for electroluminescent nanomaterials.